CASL-U-2015-0265-000

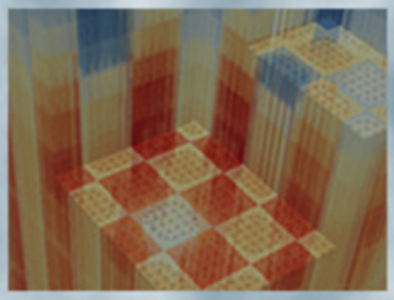

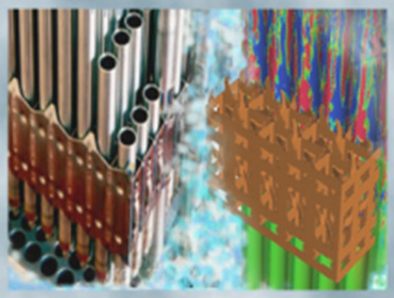

Initial BWR Modeling Capability for MPACT

Brendan Kochunas Daniel Jabaay

Andrew Fitzgerald Thomas Downar

University of Michigan

Scott Palmtag

Core Physics, Inc.

July 31, 2015

REVISION LOG

Revision	Date	Affected Pages	Revision Description
0	7/31/2015	All	Initial version

Document pages that are:

Export Controlled _____None_____

IP/Proprietary/NDA Controlled_____None_____

Sensitive Controlled_____None_____

Requested Distribution:

To:

Copy:

EXECUTIVE SUMMARY

This milestone report describes the initial effort on one of the priorities for Phase II of CASL, which is the extension of the VERA-CS LWR modeling capability to the BWR. The specific focus of the work performed here was on the extension of the deterministic neutronics code MPACT to BWR geometry. The detailed scope and objectives of this milestone were developed in a preceding milestone, L3:PHI.VCS.P10.02 for the "Initial BWR Input Specifications". As defined in the specifications, the initial capability targeted for BWR applications in VERA-CS was to be able to model (1) channel box with rounded corners, (2) wide and narrow gaps on the outside of the channel box, (3) ability to specify different void/density and outside the channel box, (4) GE Original Equipment Manufacturer (OEM) control blade design, and (5) large water rods that occupy 2x2 pin cells. Some additional second priority items from the specifications included (1) thick channel box corners, (2) "square" water rods with rounded corners (Areva ATRIUM designs), (3) 2 large water rods that together replace 7 pin cell locations (GE11 designs), and (4) large water rods that are slightly larger than 2x2 pin cells (GE9 design). Several BWR features were explicitly excluded from consideration; these exclusions were the Westinghouse SVEA water cross designs and thick-thin channel box designs. The specified BWR features were implemented in MPACT during the 5 month duration of the project and required the addition of 28,875 lines of source code and 44,895 lines of code for testing. Additionally, 24 unit tests and 25 regression tests were added to the code verification suite.

The successful completion of the milestone objectives was demonstrated using a set of BWR progression problems which were defined in the specifications provided in L3:PHI.VCS.P10.02. These problems included: (1) Pin cell calculations at BWR conditions, (2) Peach Bottom assemblies with no control blades, (3) Peach Bottom assemblies with control blades, (4) Assemblies with large 2x2 water rods (generic dimensions, including both BWR and PWRs), (5) Atrium square channel box (if time permits), (6) 3-D assemblies with no feedback or control blade (stretch goal, only if time permits). No new coding features were required for the pin cell calculations, but comparison of the results of these cases with Monte Carlo calculations enabled the testing of the cross section library using BWR fuel rod dimensions and void conditions. Several deficiencies were revealed in the cross sections library, particularly at high void conditions, and will be addressed in future work within RTM. The specifications for the Peach Bottom lattices were taken from an NEA benchmark and provided a problem to perform a preliminarily assessment of the accuracy of MPACT using a legacy BWR fuel assembly design. The reference simulations for the lattices were calculated using KENO and included a total of 6 lattice types over a variety of conditions. The comparison with the Monte Carlo reference showed a significant reactivity bias with increasing void, which was consistent with the pin cell comparisons, and the RMS and max power differences were somewhat larger than what has been observed between MPACT and KENO for the VERA Benchmark Progression Problem 2 PWR lattices. However, the comparisons provided confidence that the BWR geometry capability was successfully implemented in MPACT. To verify some of the error attributable to the cross section library, the MPACT models were also run with the HELIOS library and compared to the KENO results. Results are also presented in the report for progress on the stretch goals including the modeling of the C/E PWR core design, the simulation of a single 3-D BWR assembly, and the simulation of an ATRIUM-10 bundle design. However, future work is required to finalize the capability for all of the stretch goals.

CONTENTS

EXECUTIVE SUMMARY iii

CONTENTS v

FIGURES vi

TABLES vii

ACRONYMS viii

ACKNOWLEDGEMENTS ix

1. INTRODUCTION 1
   1.1 Summary of BWR Technology 1
   1.2 Scope and Objectives 4

2. BWR MODELING CAPABILITY 6
   2.1 New VERA Input Processing Features 6
   2.2 New Reactor Geometry 6
   2.3 Rotation Capability 8
   2.4 Generalized Geometry & Mesh Capability 10
   2.5 2-D Void Map Capability 11

3. ASSESSMENT OF CROSS SECTION LIBRARY FOR BWR SYSTEMS 13

4. PRELIMINARY ANALYSIS OF PEACH BOTTOM LATTICES 14

5. DEMONSTRATION OF BWR CAPABILITY 20
   5.1 Large Water Rods 20
      5.1.1 GE Assembly Designs 20
      5.1.2 2-D C/E PWR Core 23
   5.2 2-D BWR Core Subregion 25
   5.3 Progress on ATRIUM-10 Assembly (Stretch Goal) 27
   5.4 3-D Assembly (Stretch Goal) 29
   5.5 Peach Bottom Beginning of Cycle 1 2-D (Stretch Goal) 31

6. CONCLUSIONS AND FUTURE WORK 34
   6.1 Project Outcomes 34
   6.2 Future Work 35
      6.2.1 Cross Section Data 35
      6.2.2 Methods 35
      6.2.3 Modeling 36
      6.2.4 Miscellaneous 36

REFERENCES 37

APPENDIX A - DETAILED PEACH BOTTOM LATTICE COMPARISONS 38

FIGURES

Figure 1: Illustrations of various BWR assembly designs 2
Figure 2: Control Blade Geometry Description [1] 3
Figure 3: Control Cell Illustration [2] 3
Figure 4: Typical BWR Core Map 4
Figure 5: Geometry Overlay Example 7
Figure 6: Example Input Snippet for Automatic Rotation 9
Figure 7: MPACT model illustrating example of automatic rotation 10
Figure 8: Illustration of Generalized Geometry and Meshing 11
Figure 9: Illustration of 2-D Void Map on model geometry 12
Figure 10: Peach Bottom Lattice Models for KENO and MPACT 16
Figure 11: Peach Bottom Control Blade Model for KENO and MPACT 16
Figure 12: MPACT Model Geometry for GE-9 and GE-12 like lattices 21
Figure 13: MPACT Computed Flux Distribution for GE-9 Lattice 22
Figure 14: MPACT Computed Flux Distribution for GE-12 like Lattice 22
Figure 15: Modified C/E PWR Core Model 23
Figure 16: C/E Lattice Model Geometry and Mesh 24
Figure 17: C/E PWR 2-D Model Powers 25
Figure 18: BWR Subregion Demonstration Problem 26
Figure 19: Flux Distributions for BWR subregion 27
Figure 20: BWR MOX Assembly MPACT Model from "Benchmark Problem Suite for Reactor Physics Study of LWR Next Generation Fuels" [11]. 28
Figure 21: Flux Distributions for ATRIUM-10 Lattice 29
Figure 22: Visualization of MPACT Geometry for 3-D BWR Assembly 30
Figure 23: Computed Power Distribution for 3-D BWR Assembly 31
Figure 24: Full Core Peach Bottom Unit 2 Beginning of Cycle 1 (2-D) 32
Figure 25: Peach Bottom Unit 2 BOC1 CZP Power Distribution (2-D) 33

TABLES

Table 1. Peach Bottom Lattice Simulated Conditions 14
Table 2. Averaged Unrodded Peach Bottom Lattice Simulated Conditions–ORNL P2 17
Table 3. Averaged Rodded Peach Bottom Lattice Simulated Conditions–ORNL P2 17
Table 4. Averaged Unrodded Peach Bottom Lattice Simulated Conditions–HELIOS P2 18
Table 5. Averaged Rodded Peach Bottom Lattice Simulated Conditions–HELIOS P2 18
Table 6. Averaged Unrodded Peach Bottom Lattice Simulated Conditions–ORNL TCP0 18
Table 7. Averaged Rodded Peach Bottom Lattice Simulated Conditions–ORNL TCP0 18
Table 8. Project Metrics 34

ACRONYMS

2-D	Two-Dimensions
3-D	Three-Dimensions
AMA	Advanced Modeling Applications
BWR	Boiling water reactor
CASL	Consortium for Advanced Simulation of Light Water Reactors
CFD	Computational fluid dynamics
CTF	COBRA-TF subchannel thermal-hydraulics code
CZP	Cold Zero Power
EPRI	Electric Power Research Institute
FA	Focus Area
GE	General Electric
HFP	Hot Full Power
HPC	High-performance computing
HZP	Hot Zero Power
INL	Idaho National Lab
LWR	Light water reactor
LWRS	Light Water Reactor Sustainability
MOC	Method of characteristics
MPACT	Michigan parallel characteristics transport code
OEM	Original Equipment Manufacturer
ORNL	Oak Ridge National Laboratory
PCM	Percent mille (10-5)
PHI	Physics Integration
PWR	Pressurized water reactor
RSICC	Radiation Safety Information Computational Center
RTM	Radiation Transport Methods
T/H	Thermal-hydraulics
THM	Thermal Hydraulics Methods
UM	University of Michigan
V&V	Verification and validation
VERA	Virtual Environment for Reactor Applications
WEC	Westinghouse Electric Company

ACKNOWLEDGEMENTS

The authors would also like to acknowledge the following individuals who contributed in some way to the work reported in this document.

- Brian Ade, Oak Ridge National Lab
- Thomas Downar, University of Michigan
- Andrew Fitzgerald, University of Michigan
- Andrew Godfrey, Oak Ridge National Lab
- Daniel Jabaay, University of Michigan
- Brendan Kochunas, University of Michigan
- Scott Palmtag, Core Physics Inc.
- Srdjan Simunovic, Oak Ridge National Lab

1. INTRODUCTION

The extension of the VERA-CS LWR modeling capability to the BWR is a priority for Phase II of CASL. This milestone describes the initial effort to extend the capability of the deterministic neutronics code MPACT for BWR applications.

1.1 Summary of BWR Technology

There are currently 100 operating commercial power reactors in the US. 65 of these are PWRs and 35 are BWRS.

All of the BWR reactors in the US were designed and built by General Electric (GE). However, there are now three different fuel vendors that supply BWR fuel.

- Global Nuclear Fuel (GNF) (designs based on previous GE designs)
- Areva (designs based on previous Siemens designs), and
- Westinghouse (designs based on previous ABB designs)

Each fuel vendor has a slightly different assembly design. Some of the defining neutronics characteristics of a BWR compared to a PWR include the presence of a channel box around the fuel pins to isolate the void within each bundle, and a large water channel in the fuel pin lattice. Additionally, the first commercial reactors started with 7x7 fuel designs, but reactors have transitioned to more economical designs that use 8x8, 9x9, and 10x10 fuel. All BWRs in the US are currently using 10x10 fuel designs, but some international reactors still use 9x9 designs. There are also several other minor differences in the channel box design between modern and historical designs and vendors; such as "thick-thin" channel boxes and channel boxes with thick corners. Some of the modern and historical designs of various bundles are illustrated in Figure 1.

Another distinguishing feature of a BWR core is the control blade design shown in Figure 2. Rather than having the rodlets of the control rod inserted into guide tubes in the assembly as in a PWR, the control blade is cruciform in shape and is inserted between neighboring assemblies as shown in Figure 3.

In a BWR, the assembly pitch is also about 3/4 that of a PWR, and the number and arrangement of the assemblies within the core also differs from a PWR. At the core level, BWR assemblies are arranged in different rotational orientations around a control rod in a control cell as shown in Figure 3. Finally, the operating conditions within a BWR are significantly different than in a PWR. BWRs operate at much lower pressure relative to a PWR, and boiling occurs in the pressure vessel, rather than in a steam generator as in a PWR.

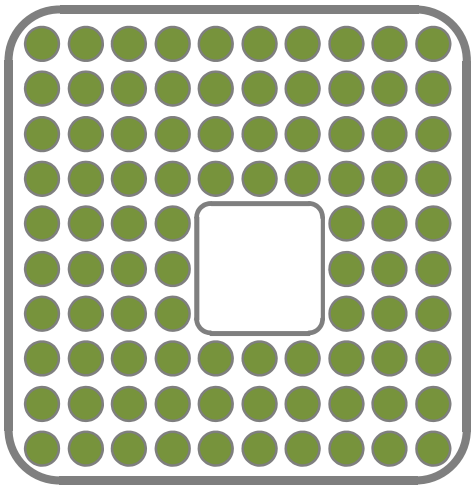

(b) ATRIUM 10 (Areva)

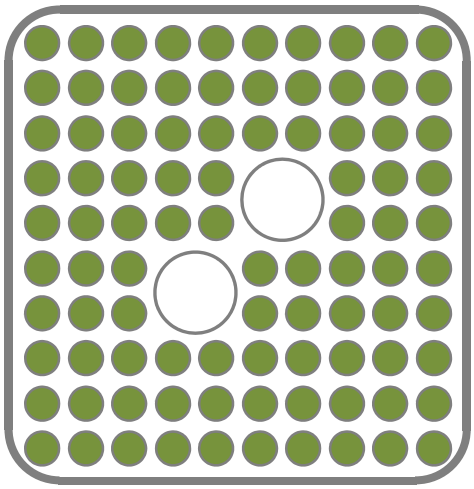

(b) GE12 (GNF)

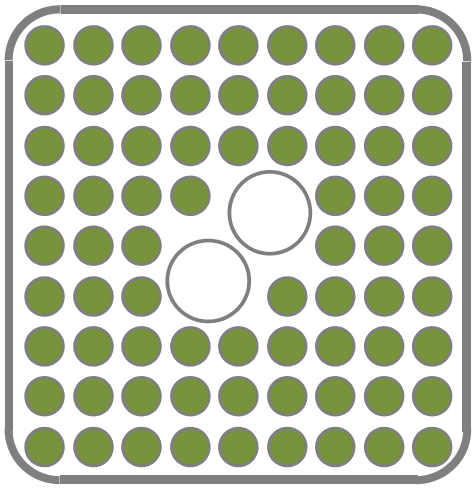

(c) GE11 (GNF)

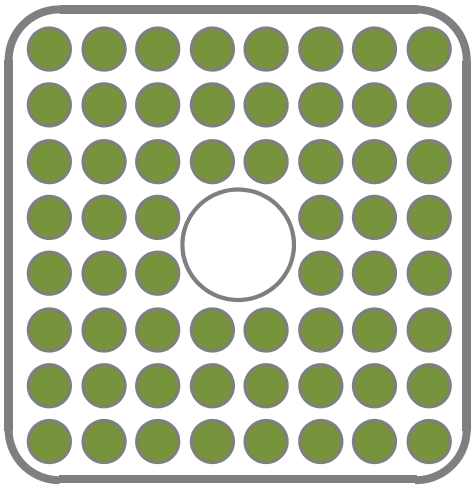

(d) GE9

Figure 1: Illustrations of various BWR assembly designs

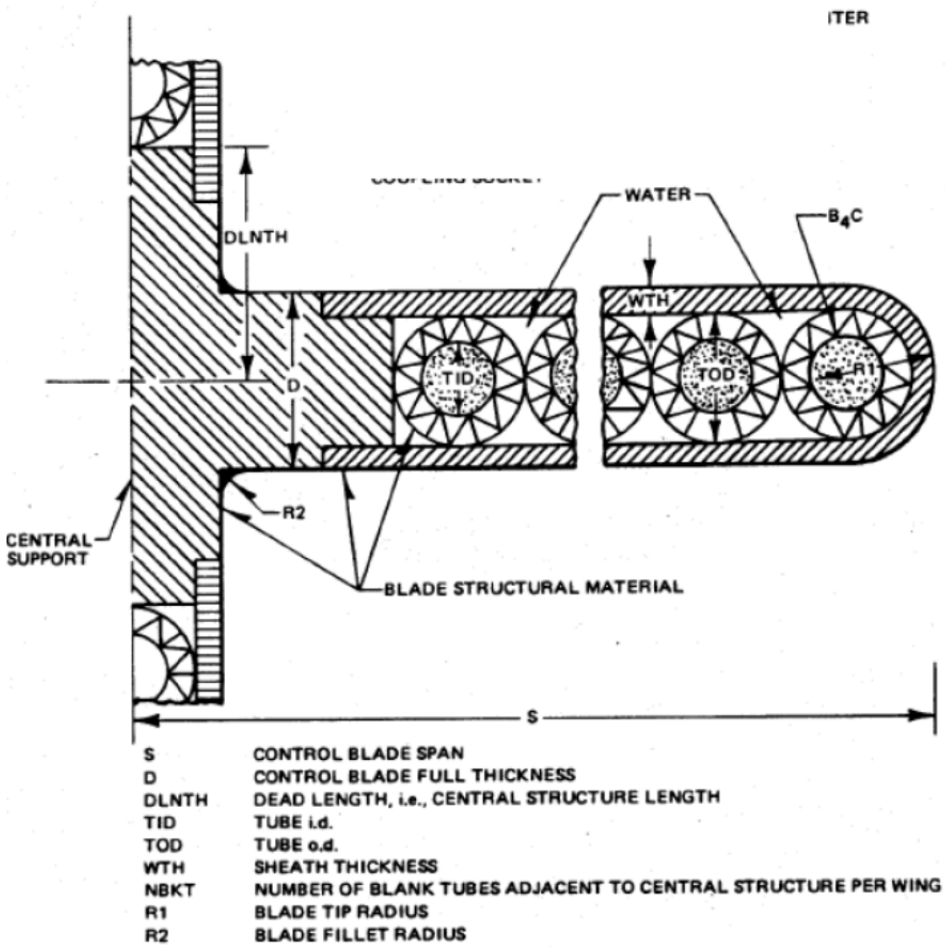

Figure 2: Control Blade Geometry Description [1]

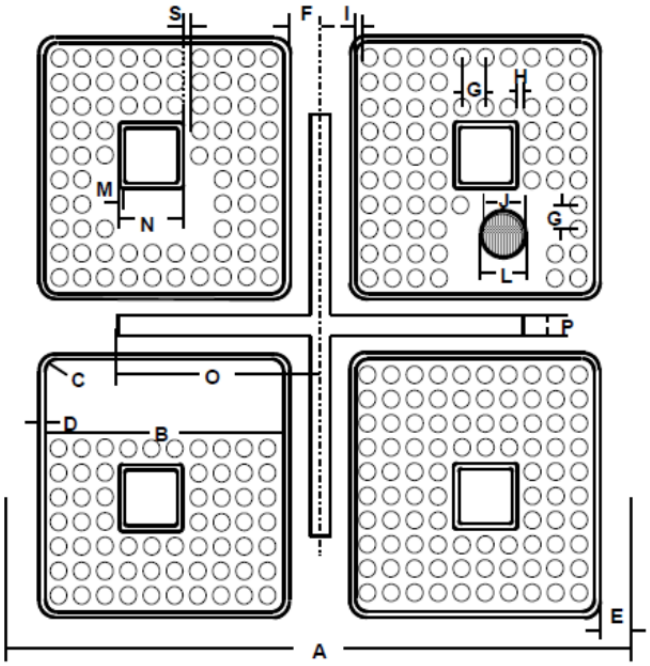

Figure 3: Control Cell Illustration [2]

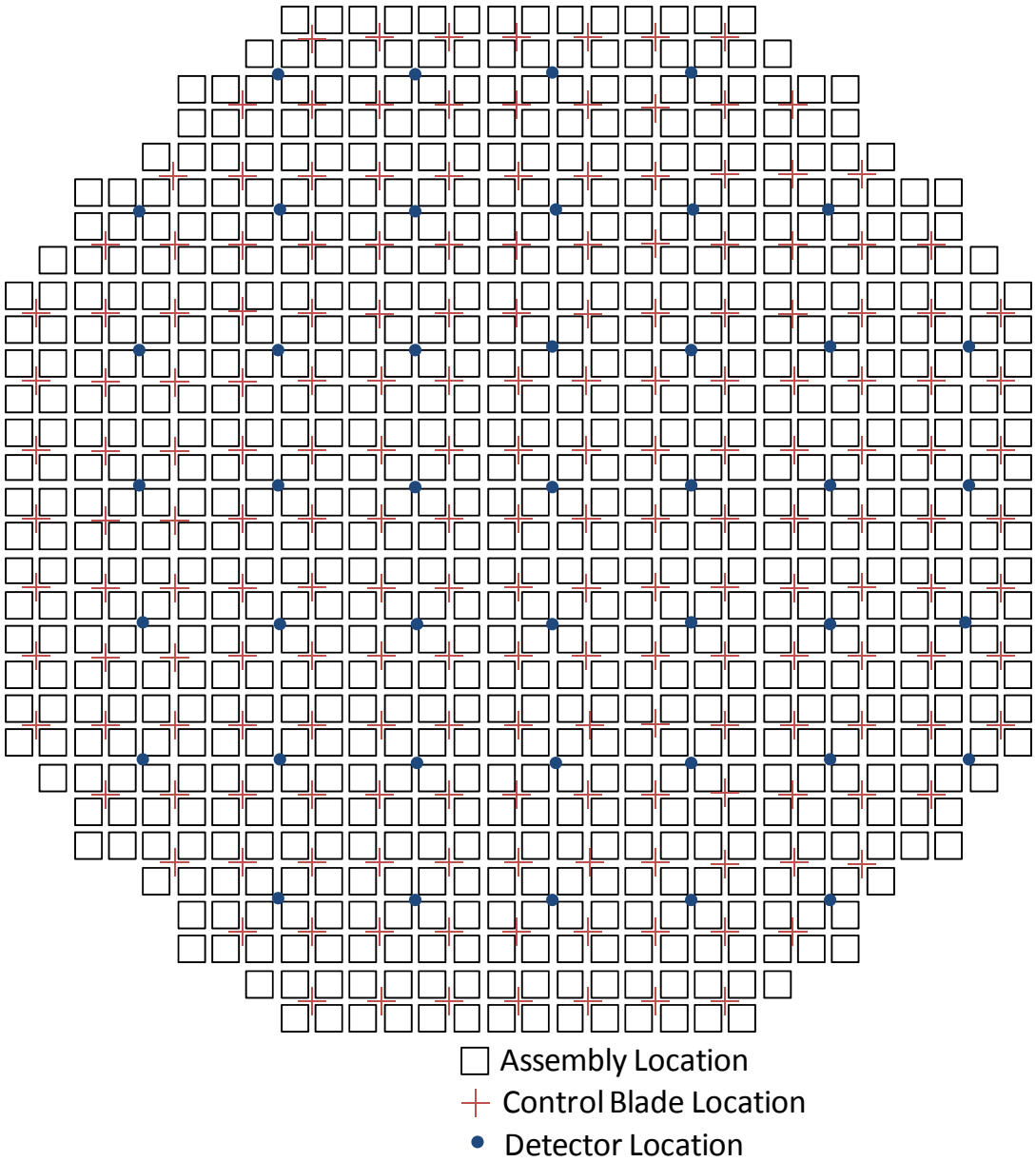

Figure 4: Typical BWR Core Map

1.2 Scope and Objectives

The scope and objectives of this milestone were developed in a preceding milestone, L3:PHI.VCS.P10.02 for the "Initial BWR Input Specifications" [3]. This section summarizes the capability outlined in the previous milestone. From specifications, the initial capability targeted for support in VERA-CS was completed. The list of this initial capability is:

- Channel box with rounded corners
- Wide and narrow gaps on the outside of the channel box
- Ability to specify different void/density and outside the channel box
- GE Original Equipment Manufacturer (OEM) control blade design
- Large water rods that occupy 2x2 pin cells

Additional support for lower priority items that were not completed from the initial specification include:

- Thick channel box corners
- "Square" water rods with rounded corners (Areva ATRIUM designs)
- Two large water rods that together replace 7 pin cell locations (GE11 designs)
- Large water rods that are slightly larger than 2x2 pin cells (GE9 design)

The BWR features that are explicitly not included as a part of this scope include:

- Westinghouse SVEA water cross designs
- Thick-thin channel box designs
- Non-OEM control blade designs
- Diagonal symmetry
- BWR detectors
- Mixed configurations of assemblies that have different numbers of rods (e.g. 8x8 assemblies and 10x10 assemblies in the same problem)

A set of BWR progression problems was proposed to demonstrate the successful completion of these objectives which included:

1. Pin cell calculations at BWR conditions. There is no new code features needed for this step, but tests the cross section library using BWR fuel rod dimensions and void.
2. Peach Bottom Assemblies with no control blades
3. Peach Bottom Assemblies with control blades
4. Assemblies with large 2x2 water rods (generic dimensions, for both BWR and PWRs)
5. Atrium square channel box (stretch goal)
6. 3-D assemblies with no feedback or control blade (stretch goal)
7. 2-D BWR core (stretch goal)

The remainder of the report is organized as follows: Section 2 summarizes the capability added in support of BWR applications. Section 3 discusses progression problem 1 for the 2-D pin cells. The Peach Bottom assemblies of progression problems 2 and 3 are analyzed in Section 4. Section 5 provides evidence demonstrating the capability to perform progression problems 4 through 7. However, these demonstration problems (4 through 7) do not include detailed neutronics comparisons to reference Monte Carlo solutions because of ongoing work to address known issues with the neutron cross section library used by MPACT. In section 4 there are preliminary comparisons between Monte Carlo and MPACT for the Peach Bottom lattices to provide evidence that the new modeling capability is functioning accurately insofar as the cross section library allows.

2. BWR MODELING CAPABILITY

The majority of the challenges in developing the initial BWR capability in MPACT involve the development of new geometry modeling capability. The features that must be added fall into roughly three categories:

- Input processing for new geometry features
- Addition of new geometry models
- Automated meshing of new geometry

Therefore the majority of the work described in this milestone involved input processing and development of new discretization methods, not necessarily the development of new reactor physics methods.

2.1 New VERA Input Processing Features

Several aspects of BWR design required additions to the VERA input specification and processing. The vast majority of BWR geometry can be input in the same way as a PWR. For instance, a BWR still has an assembly map, which is made of lattices and pin cells, etc. However, as noted in Section 1, the principal differences arise for the following distinguishing BWR features:

- Control blade
- Channel box
- The wide and narrow gap distance
- The 2-D void map
- The large water rod

The input specifications for these features were already defined in the "BWR Input Specifications" [3] document. Appendix A in that document provided a clear set of software requirements from which an implementation was developed.

Additionally, one previous VERA input requirement for which blocks had not yet been implemented included the processing of multiple `[ASSEMBLY]` blocks which was implemented as a part of this work. The primary reason for this feature is that in the VERA input, each assembly type may have only a narrow-wide gap and channel box defined. In operating BWR's, such as Peach Bottom Unit 2, the core design may contain identical fuel descriptions enclosed in different channel boxes which thus necessitates this additional input processing feature.

2.2 New Reactor Geometry

The creation of the BWR core geometry was also facilitated by additions to several existing objects within MPACT, which included new channel box geometry and control blade geometry objects. An array of control blade objects are initialized when modeling a BWR and blades are present in the input. Assembly geometry now specifies the wide and narrow gap, while before it needed only the gap for PWRs. This change resulted in other modifications in the code where the gap was assumed to be uniform. The assembly geometry also now has a channel box geometry pointer.

The channel box and control blade geometries have subroutines that allow for the generation of their respective geometry and parameters to mesh that geometry. Other subroutines were added that overlay the channel box and control blade geometry onto lattices if the object is present. An example of this input along with an illustration of the overlay process is shown in Figure 5.

```
[ASSEMBLY]
  npin   8
  ppitch 1.6256          ! pin pitch - does not include channel gaps

!*** 80 mil design
  gap    0.9525 .47498   ! wide and narrow channel gap (cm)
  channel_box  zirc4 0.2032 0.9652 0.0 0.0   ! channel dimensions
!... Define fuel loading in lattice ...
[CONTROL]
  title "GE OEM Control Blade"
  npin 8
  stroke  365.76 48    ! 6in step size and 48 steps
  mat ss304 8.0
  mat b4c   1.74
  cell TUBE 0.17526 0.23876 / b4c ss304  ! BWR Blade rodlet
!       ntube     span   th       rad    sheath    wing   mat
  blade 21 TUBE 12.3825 0.79248 0.39624 0.14224  1.98501  ss304

!*** TUBE must be included in map, or it will be excluded from
parameter list
  rodmap  EMPTY
     TUBE
     - -
     - - -
     - - - -
     - - - - -
     - - - - - -
     - - - - - - -
     - - - - - - - -
  axial BLADE 0.0 EMPTY 1.0
```

(a) Example VERA input for control blade and lattice with channel box

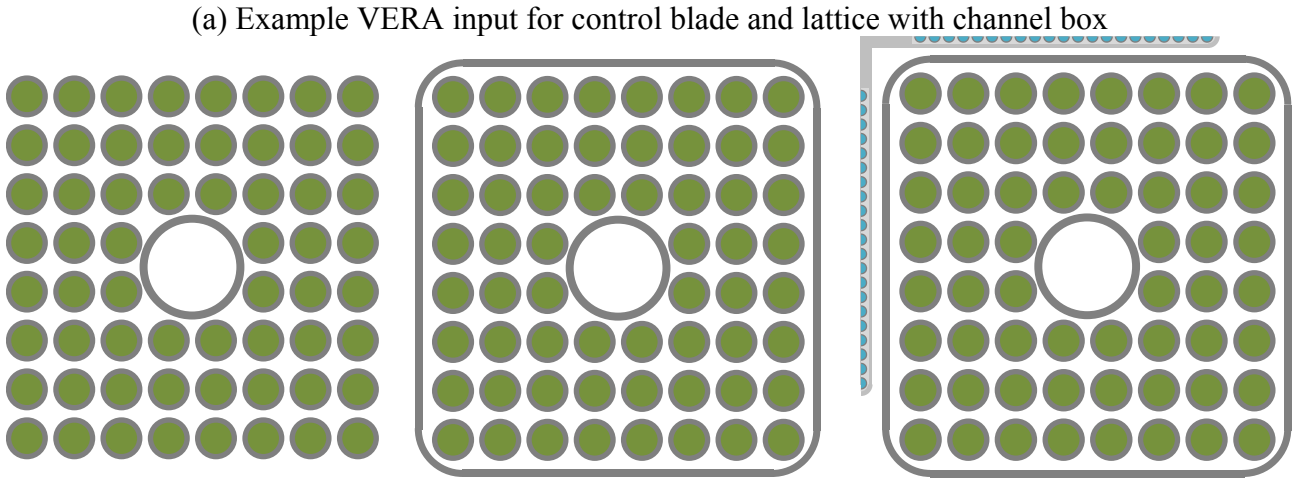

(b) GE 9 (c) GE 9 w/ Channel Box (d) Rodded GE 9 w/ Channel Box

Figure 5: Geometry Overlay Example

A "bare" lattice map is created in (b), then channel box geometry is overlaid onto the peripheral pins in (c), and lastly the blade is overlaid on the north and west facing pins in (d). Each geometry

component is overlaid independently of the others. This methodology simplifies the coding process for setting up the geometry in the event there are multiple types of control blades and channel boxes. This overlay process is performed for all unique lattice types in the core.

2.3 Rotation Capability

In a BWR, each assembly location has a fixed orientation (or rotation) relative to the nearest control blade. However, in some PWRs it is possible to change rotation of an assembly within a given location. Therefore, the VERA input allows for the user to define a "rotation map". In BWR simulations, the user is prohibited from supplying this map in the input, and instead the map is automatically generated by the code.

Additionally, the user should specify all assembly geometry in the orientation of the south-east assembly position of the control cell as shown in Figure 3. The code will then automatically rotate the geometry/mesh to the correct orientation since it is practically a certainty that a single assembly type will appear in each of the four orientations within the core.

To illustrate this feature, consider the following sample input which defines the Type 1 Peach Bottom lattice and a 6x6 subregion of assemblies within the core:

```
[CORE]

!... other core inputs

reactor_type BWR

core_shape
  1 1 1 1 1 1
  1 1 1 1 1 1
  1 1 1 1 1 1
  1 1 1 1 1 1
  1 1 1 1 1 1
  1 1 1 1 1 1

                           !*** Rotation map determined by code
assm_map                   !rotate_map
  A1 A1 A1 A1 A1 A1        ! 2 3 2 3 2 3
  A1 A1 A1 A1 A1 A1        ! 1 0 1 0 1 0
  A1 A1 A1 A1 A1 A1        ! 2 3 2 3 2 3
  A1 A1 A1 A1 A1 A1        ! 1 0 1 0 1 0
  A1 A1 A1 A1 A1 A1        ! 2 3 2 3 2 3
  A1 A1 A1 A1 A1 A1        ! 1 0 1 0 1 0

[ASSEMBLY]
 title "Peach Bottom Fuel Type 1"
 npin 7
 ppitch 1.87452
 gap 0.9525 0.47498

 channel_box zirc4 0.2032 0.9652 0.0 0.0

 fuel U133 10.34 94.5 / 1.33
 fuel U071 10.34 94.5 / 0.71

 cell 1 0.61849 0.63373 0.71501 / U133 he zirc2
 cell 2 0.61849 0.63373 0.71501 / U071 he zirc2

 lattice LAT1
  2  1  1  1  1  1  1
  1  1  1  2  1  1  1
  1  1  2  2  2  2  1
  1  2  2  2  2  2  1
  1  1  2  2  2  2  1
  1  1  2  2  2  1  1
  1  1  1  1  1  1  1

 axial A1 0.0 LAT1 1.0
```

Figure 6: Example Input Snippet for Automatic Rotation

From this input, the resulting model produced by MPACT is illustrated in Figure 7; note that this determines placement of the narrow and wide gaps.

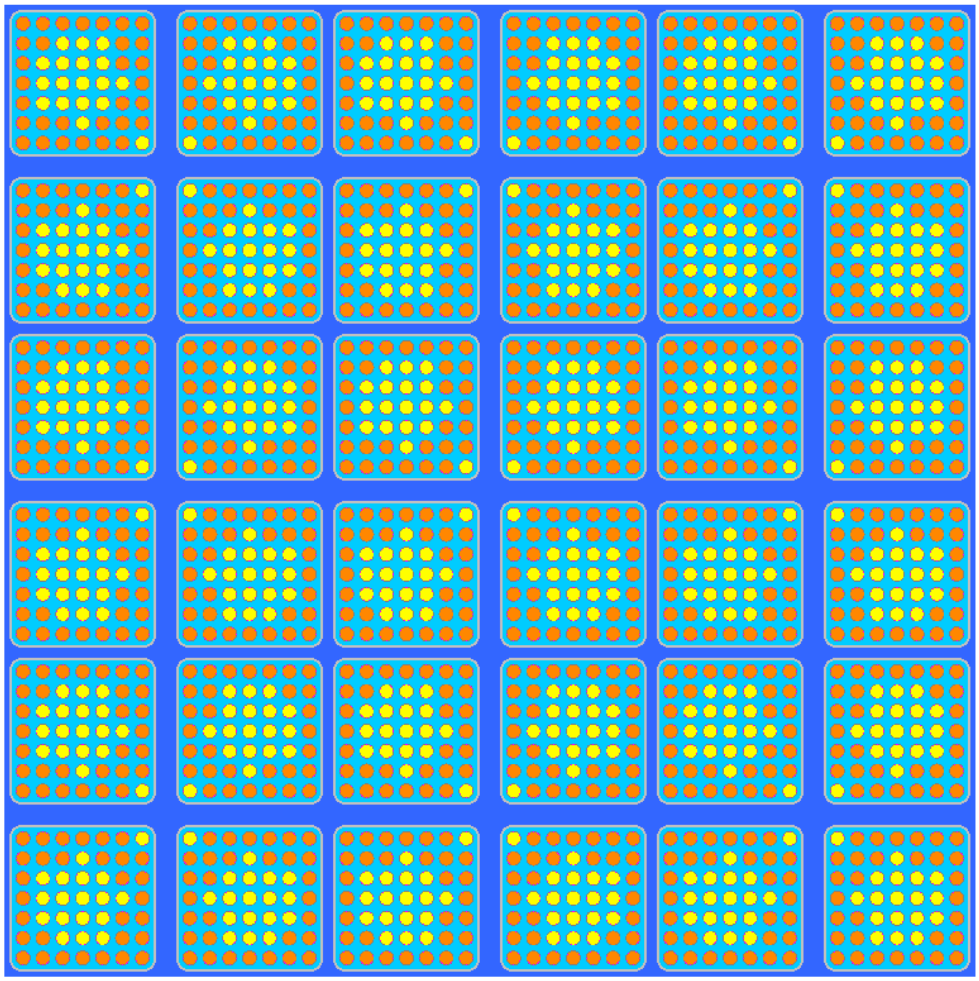

Figure 7: MPACT model illustrating example of automatic rotation

2.4 Generalized Geometry & Mesh Capability

The meshing strategy within MPACT is to first lay down a Cartesian mesh for the pin cells in a lattice. Then the flat source region mesh is developed for each pin cell based on its geometry. For the PWR application the pin cell could essentially be another Cartesian mesh, or contain a set of concentric circles. This meshing strategy is not sufficient for representing the more complicated structures of a BWR that include the control blade and rounded channel boxes. Therefore a more general meshing capability was developed to treat the BWR geometry.

The approach of the new meshing capability allows for the description of boxes, circles, and circular arcs placed arbitrarily within a pin cell. These geometric volumes can then be overlayed on top of each other totally arbitrarily to produce the correct pin cell geometry. The resulting set of volumes produced by the overlay is then meshed using similar meshing parameters as in PWRs; for example, the number of radial subdivisions for circles and number of x and y divisions for boxes. Furthermore, mesh lines may be placed arbitrarily over the combinatorial geometry to further define mesh regions. Figure 8 illustrates how this new generalized meshing capability works.

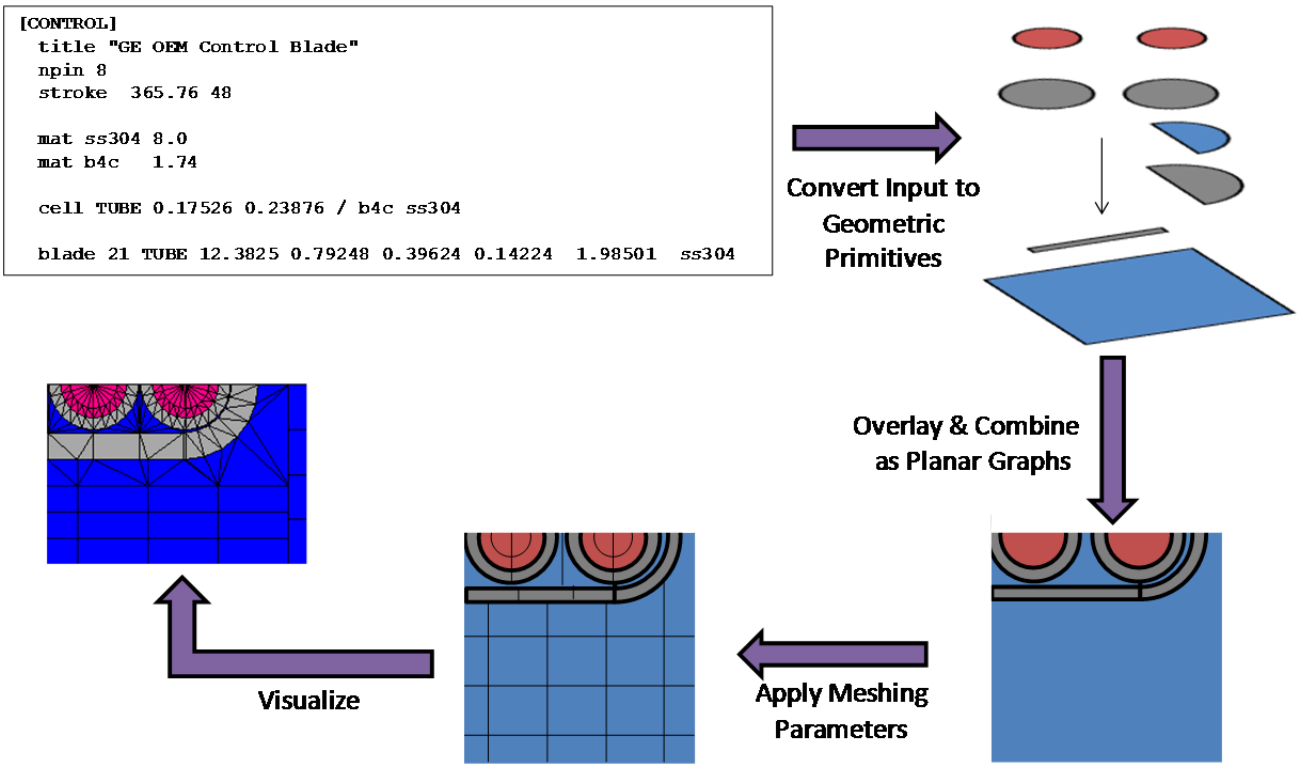

Figure 8: Illustration of Generalized Geometry and Meshing

All of this complexity is transparent to the user, and essentially allows for the physical representation of any 2-D geometry. As an underlying capability, it will be able to support the geometry features not yet implemented which includes: thick-thin channel boxes, GE11 water rods, and SVEA water crosses, thick channel box corners, and fully explicit spacer grids. The primary work remaining to develop these capabilities is to first define their input format, and then to add the necessary processing to describe the input parameters into the necessary data needed for the generalized pin mesh.

In addition to the generalized geometry and meshing capability, the visualization capability in MPACT needed to be updated to be able to edit and display the more geometrically complex BWR models.

2.5 2-D Void Map Capability

The initial BWR capability is targeted for 2-D problems without feedback. To better evaluate this capability for the realistic conditions required in the future, an initial capability to specify a map of the coolant void distribution by assembly was developed and implemented.

The calculation of the coolant density is performed using Eq. (1).

$$\rho_{cool} = \left(1 - \frac{\alpha}{100\%}\right)\rho_{liquid} + \frac{\alpha}{100\%}\rho_{vapor}, \tag{1}$$

where α is the percent void, and ρ_{liquid} and ρ_{vapor} correspond to the liquid and vapor densities of water, respectively, at saturation conditions for the user specified system pressure. The liquid and vapor densities are obtained through linear interpolation of tabulated densities at saturation

conditions, where the lookup is provided by either temperature or pressure. The liquid and vapor densities are tabulated in temperature from 274 K up to 647 K in 1 K increments, effectively covering the full temperature range for saturation conditions. The tabulated data was obtained from the NIST database [4]. Additionally, the temperature of the coolant can be specified such that it does not correspond to saturation conditions for the given pressure; while this is non-physical, it is necessary to enable numerical comparisons with Monte Carlo reference solutions.

Once the coolant density is obtained for a given assembly, the associated number densities for water are updated on the mesh for all coolant regions within the channel box. Figure 9 illustrates how the void distribution is applied to the problem geometry.

```
[STATE]
    void
      60.0 20.0
      40.0  0.0
```

(a) VERA Input Void Map Example

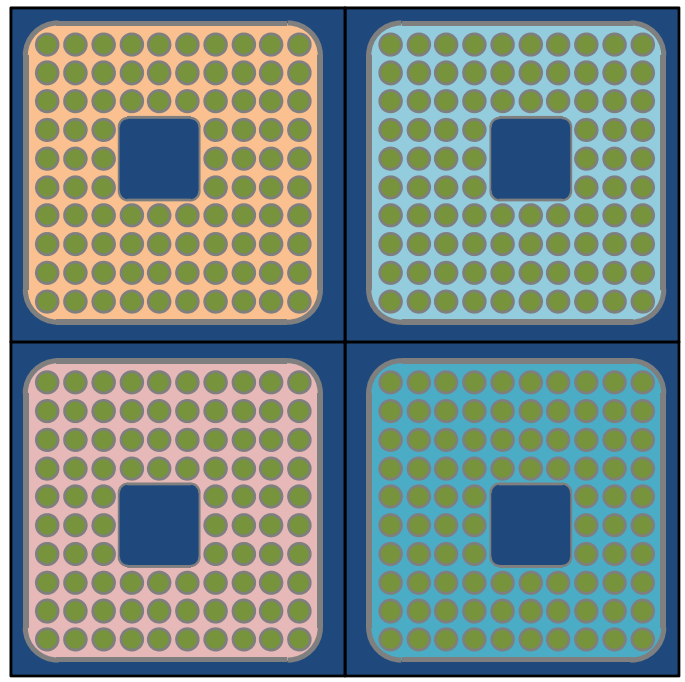

(b) Application of Void Map to Model

Figure 9: Illustration of 2-D Void Map on model geometry

It is also worth noting that the density of the moderator in the bypass flow regions is obtained automatically using the liquid density computed from the tabulated saturated water properties using the system pressure.

3. ASSESSMENT OF CROSS SECTION LIBRARY FOR BWR SYSTEMS

The cross section library used for the first phase of CASL was generated specifically for PWR systems. With the addition of BWR modeling, there has been effort to re-examine the suitability of the current cross section library for its applicability to BWR analysis. The current multi-group cross section library was tested on BWR pin geometry. Comparisons were performed between MCNP and MPACT for simple pin cell calculations across a variety of void fractions and pin cells, and large errors were identified for voided cases.

During the investigation of the voided cross sections, two correlations that demonstrate the deficiencies of the current cross section library were identified. The first correlates an increasing error between MPACT and MCNP as a function of decreasing fuel radius. The second proportionally correlates the error to the void fraction. Because of these differences, further work has been initiated to investigate and resolve cross section library deficiencies. Nonetheless, the existing MPACT library was used to assess the BWR functionality developed in this milestone by comparing to a Monte Carlo solution as a reference.

4. PRELIMINARY ANALYSIS OF PEACH BOTTOM LATTICES

The specifications for the Peach Bottom lattices analyzed in this section come from [5]. The purpose of this section is to preliminarily assess the accuracy of this initial BWR capability. The reference simulations for the lattices were calculated using KENO [6]. The specification describes a total of 6 lattice types. Each lattice type is simulated over a variety of conditions. These simulated conditions are shown in Table 1.

Table 1. Peach Bottom Lattice Simulated Conditions

State	Moderator Density (g/cc)	Coolant Density (g/cc)	Non-Fuel Material Temperatures[a] (K)	Fuel Temperatures[a] (K)
Cold Zero Power[b]	0.996513	0.996513	293	293
Hot Zero Power[c]	0.736690	0.736690	600	600
Hot Full Power[c] 0% void	0.736690	0.736690	600	900

[a] Temperatures chosen to correspond with KENO cross section library evaluations.
[b] Water density computed from NIST Steam Table [4] at saturation conditions at 300K.
[c] Water density computed from NIST Steam Table [4] at saturation conditions at 1040 psia.

The geometry of the KENO and MPACT models are shown in Figure 10. The comparisons of the results of the simulations follow below.

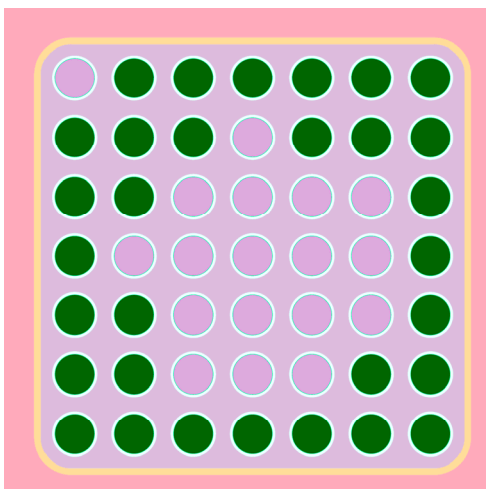

(a) Type 1 KENO Model

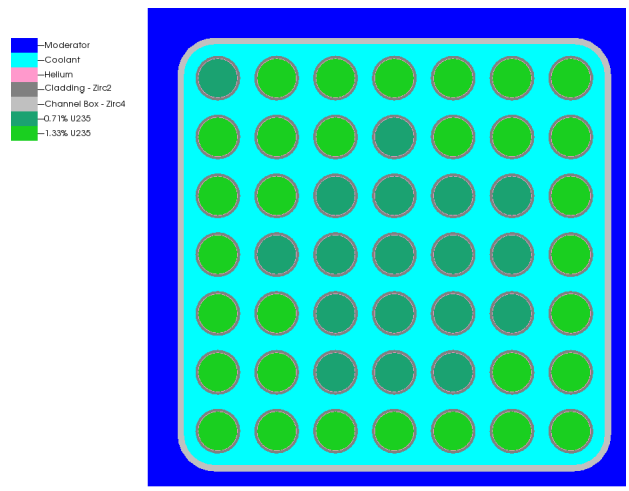

(b) Type 1 MPACT Model

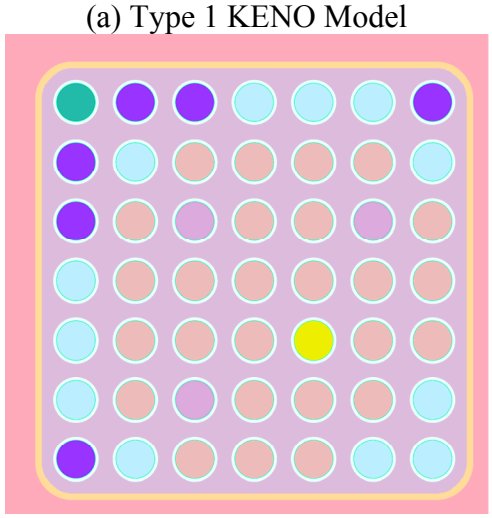

(c) Type 2 KENO Model

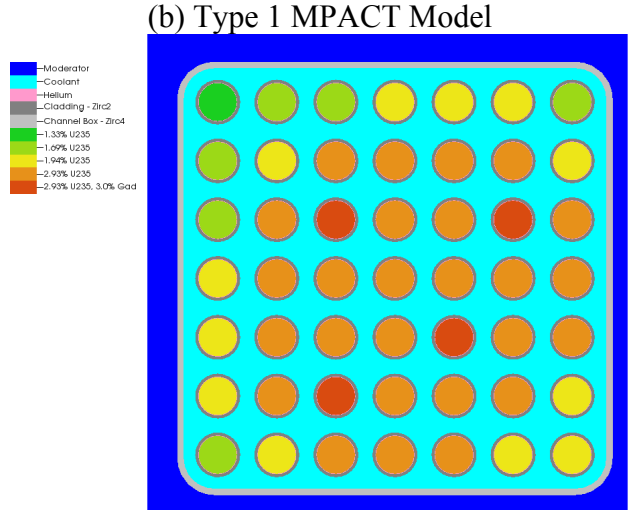

(d) Type 2 MPACT Model

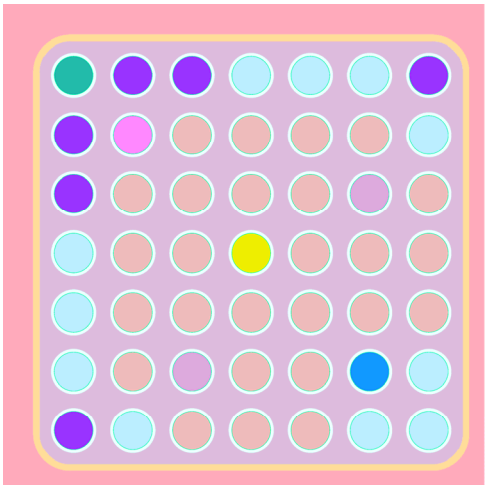

(e) Type 3 KENO Model

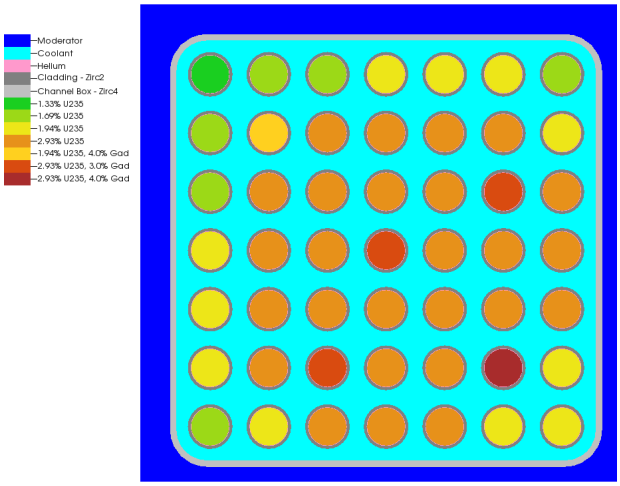

(f) Type 3 MPACT Model

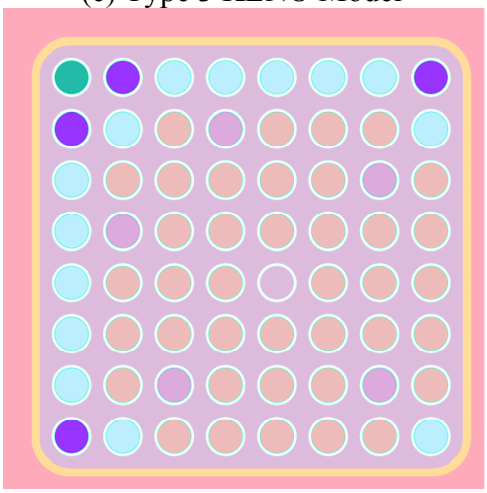

(g) Type 4 KENO Model
(100-mil channel box)

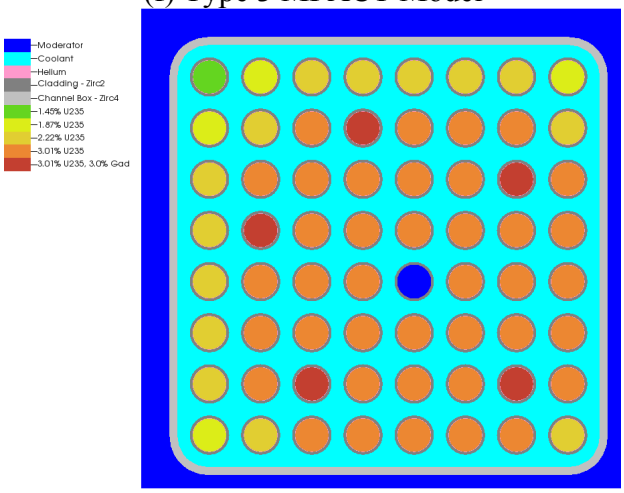

(h) Type 4 MPACT Model
(100-mil channel box)

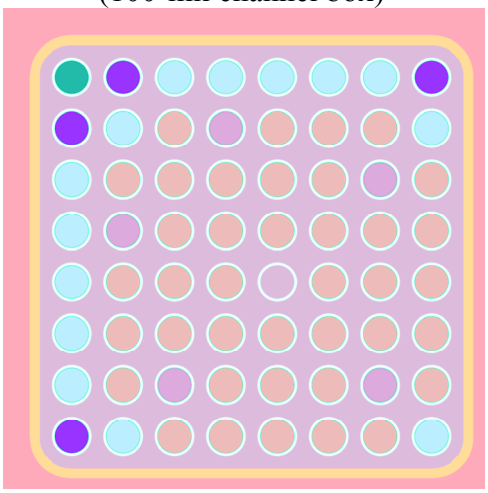

(i) Type 4 KENO Model
(120-mil channel box)

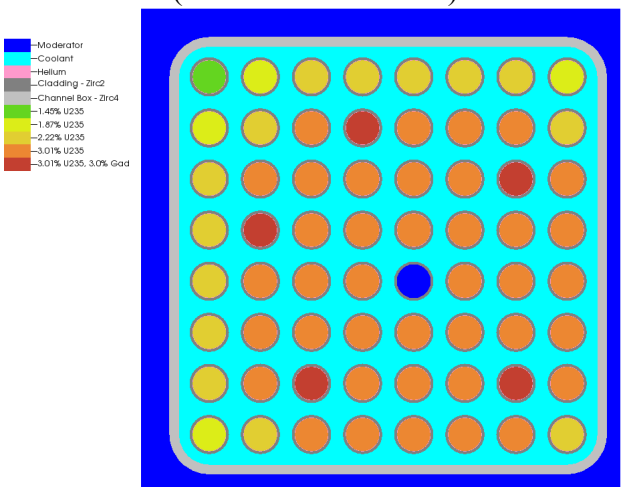

(j) Type 4 MPACT Model
(120-mil channel box)

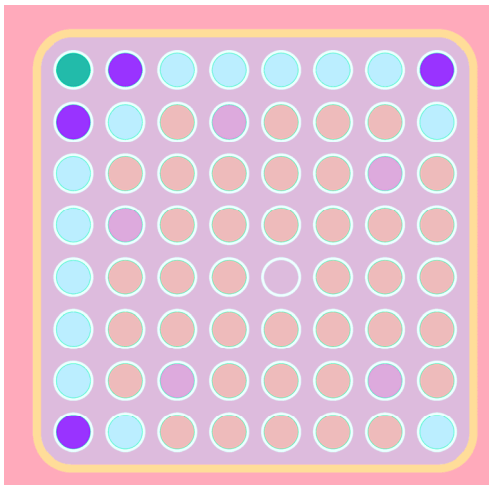

(k) Type 5 KENO Model

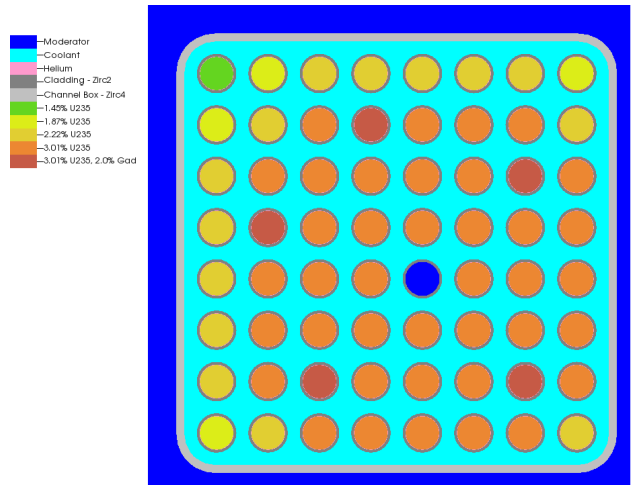

(m) Type 5 MPACT Model

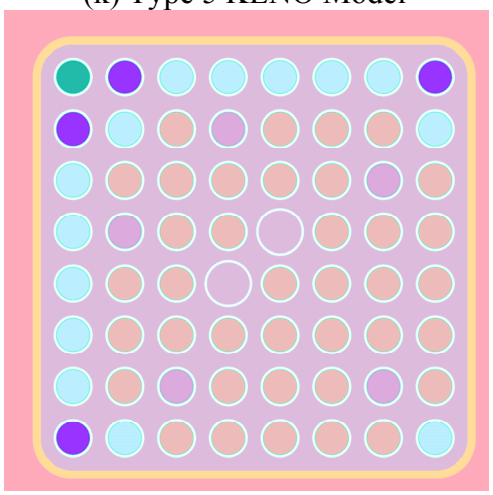

(n) Type 6 KENO Model

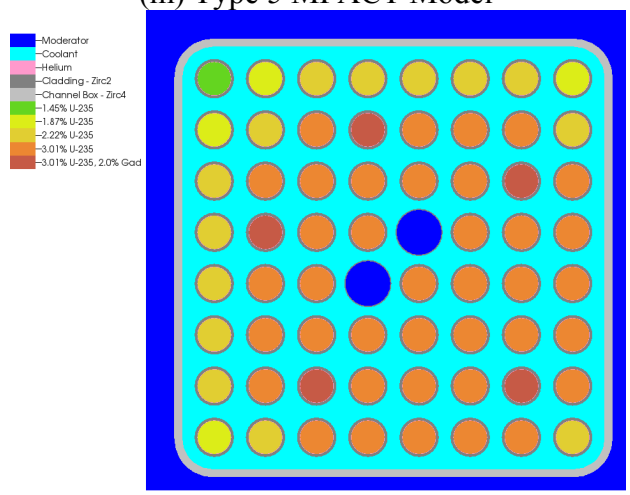

(p) Type 6 MPACT Model

Figure 10: Peach Bottom Lattice Models for KENO and MPACT

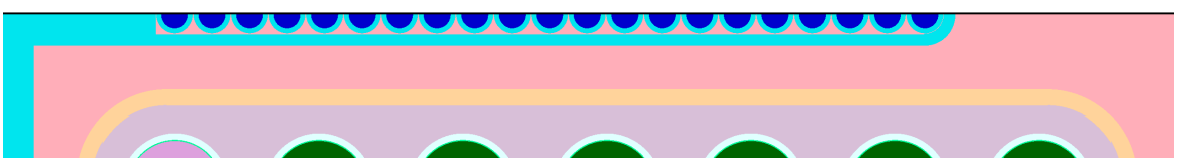

(a) North Control Blade KENO Model

(b) North Control Blade MPACT Geometry

Figure 11: Peach Bottom Control Blade Model for KENO and MPACT

The summary of the lattice comparisons are provided in Table 2 for the unrodded cases, and Table 3 for the rodded cases. Detailed comparisons of all cases are provided in Appendix A. The MPACT results used the `mpact47g_70s_v4.0_11032014.fmt` library, P2 scattering, 16 azimuthal angles per octant, 2 polar angles, the Chebyshev-Yamamoto angular quadrature, and 0.01 cm ray spacing.

Table 2. Averaged Unrodded Peach Bottom Lattice Simulated Conditions–ORNL P2

State	KENO Uncertainty	MPACT Δk-eff (pcm)[a]	Pin Power Max. Absolute Difference	Pin Power RMS
Cold Zero Power	2 pcm	170 pcm	2.39% (0.33%)	0.96% (0.18%)
Hot Zero Power	2 pcm	192 pcm	1.39% (0.27%)	0.61% (0.16%)
Hot Full Power 0% void	2 pcm	90 pcm	1.37% (0.27%)	0.60% (0.15%)
[a] Diff = ABS(MPACT – KENO)				

Table 3. Averaged Rodded Peach Bottom Lattice Simulated Conditions–ORNL P2

State	KENO Uncertainty	MPACT Δk-eff (pcm)[a]	Pin Power Max. Absolute Difference	Pin Power RMS
Cold Zero Power	2 pcm	299 pcm	1.94% (0.53%)	0.70% (0.13%)
Hot Zero Power	2 pcm	54 pcm	1.27% (0.31%)	0.50% (0.10%)
Hot Full Power 0% void	2 pcm	55 pcm	1.24% (0.31%)	0.49% (0.10%)
[a] Diff = ABS(MPACT – KENO)				

From these comparisons it is observed that the reactivity bias increases with the percent void, which is consistent with the pin cell comparisons discussed in the previous section. The average differences in these comparisons are much larger than what has been observed previously between MPACT and KENO for the PWR Problem 2 in the VERA Benchmark Progression [7]. For PWR lattices, the average reactivity difference for all problem 2 cases was 100 pcm, with a maximum of ~350 pcm. The pin power maximum absolute difference and RMS were also considerably smaller for the PWR cases with an average of 0.13% RMS and 0.29% max absolute difference. The best BWR condition was the 0% void case. The results show similar differences in reactivity and pin power RMS compared to the previous PWR studies, but a maximum local difference about 4 to 7 times higher.

Nearly all of the maximum local differences occur in the corner fuel pins by the wide-wide gap. It is possible that this difference is attributable to the spatial meshing in the gap around these fuel pins. It is well known that the spatial mesh within the gap may need to be very fine for MOC with the flat source approximation. As an activity for future work, a mesh refinement study in the gap is suggested to minimize any differences from the flat source approximation. This activity would be preceded by adding user inputs for meshing the channel box as there are none currently.

It is also observed that the differences increase when going from hot conditions to the cold conditions. This increase will require further investigation, but one possible explanation is the lack of sufficient spatial mesh in the gap near the corner fuel pins. The more dense coolant will shorten the migration length of the neutrons, thus allowing for larger thermal flux gradients, and therefore a finer mesh would be necessary to capture those steeper gradients.

The run time of MPACT using 4 threads for one of these lattices ranged from 12 to 20 minutes and 7 to 10 iterations, depending on the void. One likely reason for the longer run times is because additional transport sweeps were required for each outer iteration to ensure stability of the global iteration; compared to the typical PWR case these simulations performed a factor of ~2.5 more transport sweeps per iteration. Optimizing the CMFD stability is proposed as an area of future work.

Additionally, the MPACT models were run with the HELIOS [8] library and compared to the KENO results. These results are summarized in Table 4 and Table 5.

Table 4. Averaged Unrodded Peach Bottom Lattice Simulated Conditions–HELIOS P2

State	KENO Uncertainty	MPACT Δk-eff (pcm)[a]	Pin Power Max. Absolute Difference	Pin Power RMS
Cold Zero Power	2 pcm	86 pcm	1.41% (0.30%)	0.53% (0.12%)
Hot Zero Power	2 pcm	141 pcm	0.46% (0.14%)	0.23% (0.08%)
Hot Full Power 0% void	2 pcm	32 pcm	0.49% (0.12%)	0.26% (0.08%)
[a] Diff = ABS(MPACT – KENO)				

Table 5. Averaged Rodded Peach Bottom Lattice Simulated Conditions–HELIOS P2

State	KENO Uncertainty	MPACT Δk-eff (pcm)[a]	Pin Power Max. Absolute Difference	Pin Power RMS
Cold Zero Power	2 pcm	209 pcm	2.07% (0.36%)	0.64% (0.09%)
Hot Zero Power	2 pcm	114 pcm	0.95% (0.16%)	0.37% (0.05%)
Hot Full Power 0% void	2 pcm	61 pcm	1.00% (0.20%)	0.38% (0.06%)
[a] Diff = ABS(MPACT – KENO)				

The HELIOS library uses the same group structure as the ORNL library. The data however is based on ENDF-B6, rather than ENDF-B7 as is the case for the KENO cross sections and ORNL library. However, in spite of this difference between KENO and MPACT, the results with the HELIOS library show notably better agreement in the power distribution for the unrodded cases. When comparing the overall trends for differences in the BWR lattices using the HELIOS library versus the previous comparisons between MPACT and KENO for PWRs, the difference in the BWR application is approximately a factor of 2 on the pin powers. However, it should be noted that it is difficult to draw any definitive conclusions about the adequacy of MPACT's cross section library given the number of differences between the models. A more methodical study of the cross section library is proposed as future work.

The HELIOS library results suggest that the errors observed between KENO and MPACT with the ORNL 47-group library are due to deficiencies in the cross section library. Work is currently being done to improve these results.

Finally, the lattices were also run with the ORNL library and the transport corrected P0 (TCP0) scattering to evaluate this approximation against the P2 scattering approximation results shown in Table 2 and Table 3. The TCP0 results are summarized in Table 6 and Table 7.

Table 6. Averaged Unrodded Peach Bottom Lattice Simulated Conditions–ORNL TCP0

State	KENO Uncertainty	MPACT Δk-eff (pcm)[a]	Pin Power Max. Absolute Difference	Pin Power RMS
Cold Zero Power	2 pcm	180 pcm	2.88% (0.40%)	1.18% (0.24%)
Hot Zero Power	2 pcm	108 pcm	1.74% (0.36%)	0.71% (0.18%)
Hot Full Power 0% void	2 pcm	67 pcm	1.72% (0.37%)	0.70% (0.18%)
[a] Diff = ABS(MPACT – KENO)				

Table 7. Averaged Rodded Peach Bottom Lattice Simulated Conditions–ORNL TCP0

State	KENO Uncertainty	MPACT Δk-eff (pcm)[a]	Pin Power Max. Absolute Difference	Pin Power RMS
Cold Zero Power	2 pcm	505 pcm	3.45% (0.59%)	1.01% (0.20%)
Hot Zero Power	2 pcm	70 pcm	1.54% (0.36%)	0.51% (0.12%)
Hot Full Power 0% void	2 pcm	61 pcm	1.51% (0.35%)	0.50% (0.12%)
[a] Diff = ABS(MPACT – KENO)				

Relative to the P2 results, it is observed that the differences in the rodded cases increase significantly when using TCP0; an observation that is consistent with experiences in PWR comparisons between MPACT and KENO. Another observation is that the general trend for differences in the unrodded cases for the TCP0 results compared to KENO are almost as good as the P2 results. This trend suggests that the TCP0 approximation does not introduce significant differences for BWR problems compared to using P2. The run time of MPACT using 4 threads and TCP0 for these lattices ranged from 4 to 7 minutes and converging in 4 to 9 iterations, which is about a factor of 3 speedup over the P2 runtimes.

These results are preliminary and there remains a significant amount of analysis that should be performed for these lattices in order to fully understand the source of the differences between MPACT and KENO. This additional analysis should include assessing the effect of having slightly different number densities for water, performing systematic mesh refinement studies, and performing more detailed investigations of the reaction rates. The models developed in this work should also undergo an independent review in order to ensure consistency between MPACT and KENO, as well as consistency with the specifications in [5].

5. DEMONSTRATION OF BWR CAPABILITY

In this section the new capability is demonstrated for a variety of target applications. These applications include the objectives for the simulations defined in [3], and discussed in Section 1. In addition to the milestone objectives, evidence is presented on current progress towards the stretch goals that were outlined in Section 1. Finally, because the focus here is on demonstration, there are no comparisons to reference solutions evaluating the accuracy of the simulation. The purpose is rather to show evidence of the capability and provide some information about code performance at present.

5.1 Large Water Rods

Large water rods not only occur in several BWR assembly designs, but also in the C/E PWR plant designs. Therefore we demonstrate this capability for the designs that are slightly modified from the GE9 and GE12. For the PWR we demonstrate the capability for a 2-D core design similar to the reactor simulated in year 1 of CASL [9].

5.1.1 GE Assembly Designs

Two GE lattice designs were simulated to demonstrate the large water rod capability. The first was a GE-9, where the specification comes from [10]. The second is a GE-12 like design where the fuel loading pattern specification was adapted from an Atrium-10 design [2], and the large water rod inner diameter is chosen arbitrarily. The geometry of the GE-9 and GE-12 problems is shown in Figure 12. The calculated flux distribution for specific groups is shown in Figure 13 and Figure 14 for the GE-9 and GE-12 respectively.

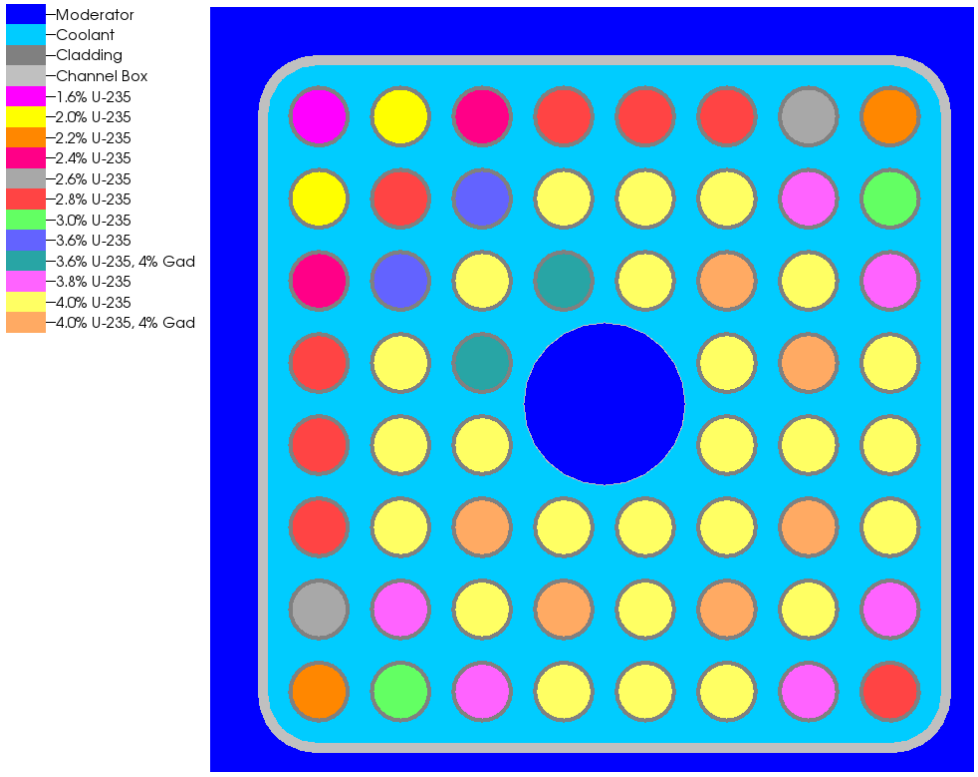

(a) GE-9 Lattice Model Geometry

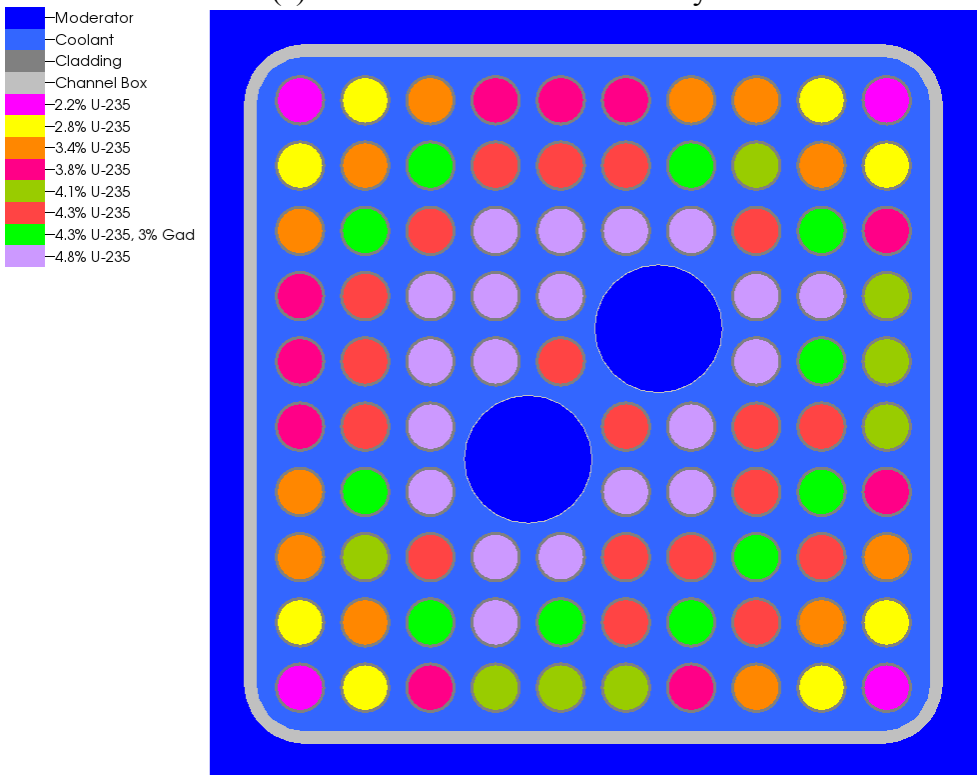

(c) GE-12 Lattice Model Geometry

Figure 12: MPACT Model Geometry for GE-9 and GE-12 like lattices

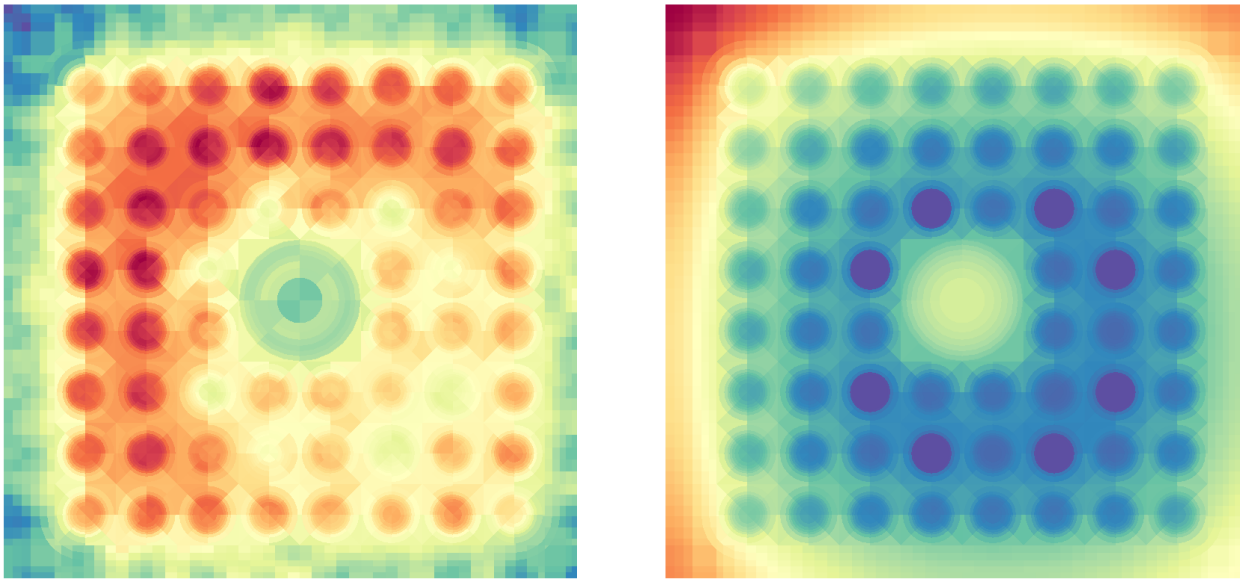

(a) Fast Flux (20 MeV - 6.0653 MeV) (b) Thermal Flux (< 0.012396 eV)

Figure 13: MPACT Computed Flux Distribution for GE-9 Lattice

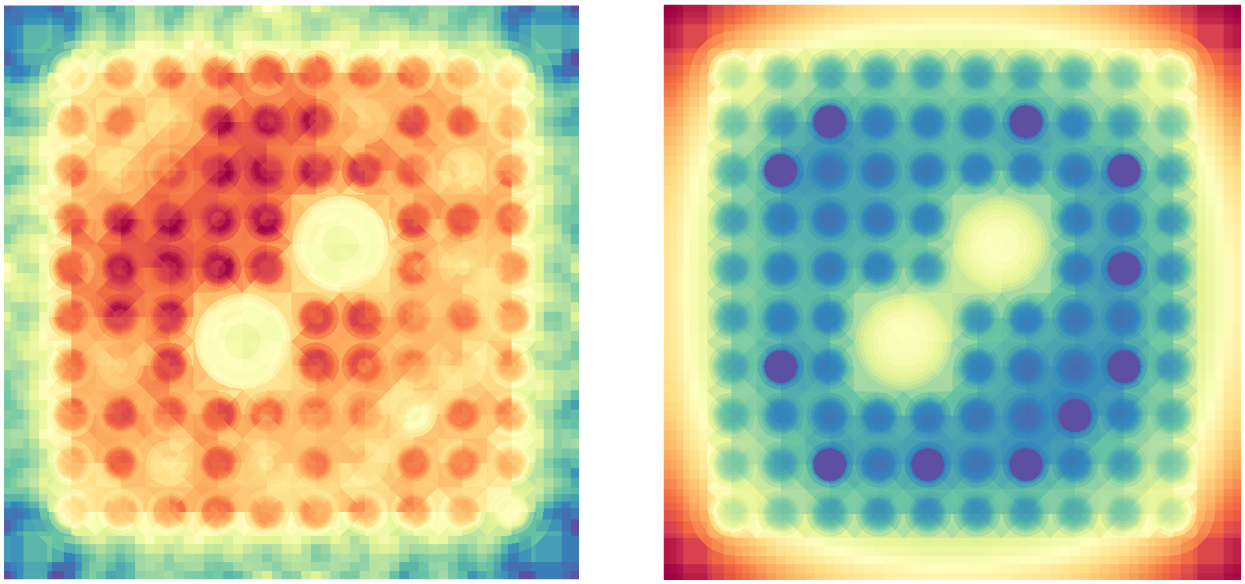

(a) Fast Flux (20 MeV - 6.0653 MeV) (b) Thermal Flux (< 0.012396 eV)

Figure 14: MPACT Computed Flux Distribution for GE-12 like Lattice

Since these simulations were performed for demonstration purposes, the mesh used here is very likely not fully converged, and thus a finer spatial mesh and MOC mesh would be needed to obtain reference quality solutions. These models used 5 equi-volume rings in the fuel, and 7 equi-volume rings in the water rods. The MOC discretization used 0.05 cm spacing, 8 azimuthal angles and 2 polar angles per octant with the Cheybyshev-Yamamoto quadrature. The `mpact47g_70s_v4.0_11032014.fmt` library was used with transport corrected P0 scattering. Simulated conditions correspond to hot full power at 40% void. Each calculation was performed with just 4 threads on a workstation, and the run times were 47 s and 62 s for the GE-9 and GE-12, respectively. The convergence criteria for the eigenvalue and flux were set to 1.0e-6 for both models and these criteria were reached after 6 and 5 iterations, respectively.

5.1.2 2-D C/E PWR Core

This design was adapted from [9]. In the original plant the peripheral row of assemblies is off-set by a half-assembly pitch. This feature is a modeling capability that is not yet available in the VERA input. Therefore, the assembly layout is modified so that the peripheral row has 5 assemblies in a structured grid. The full core geometry model in MPACT is shown in Figure 15. The model geometry for the individual lattice types and mesh is shown in Figure 16.

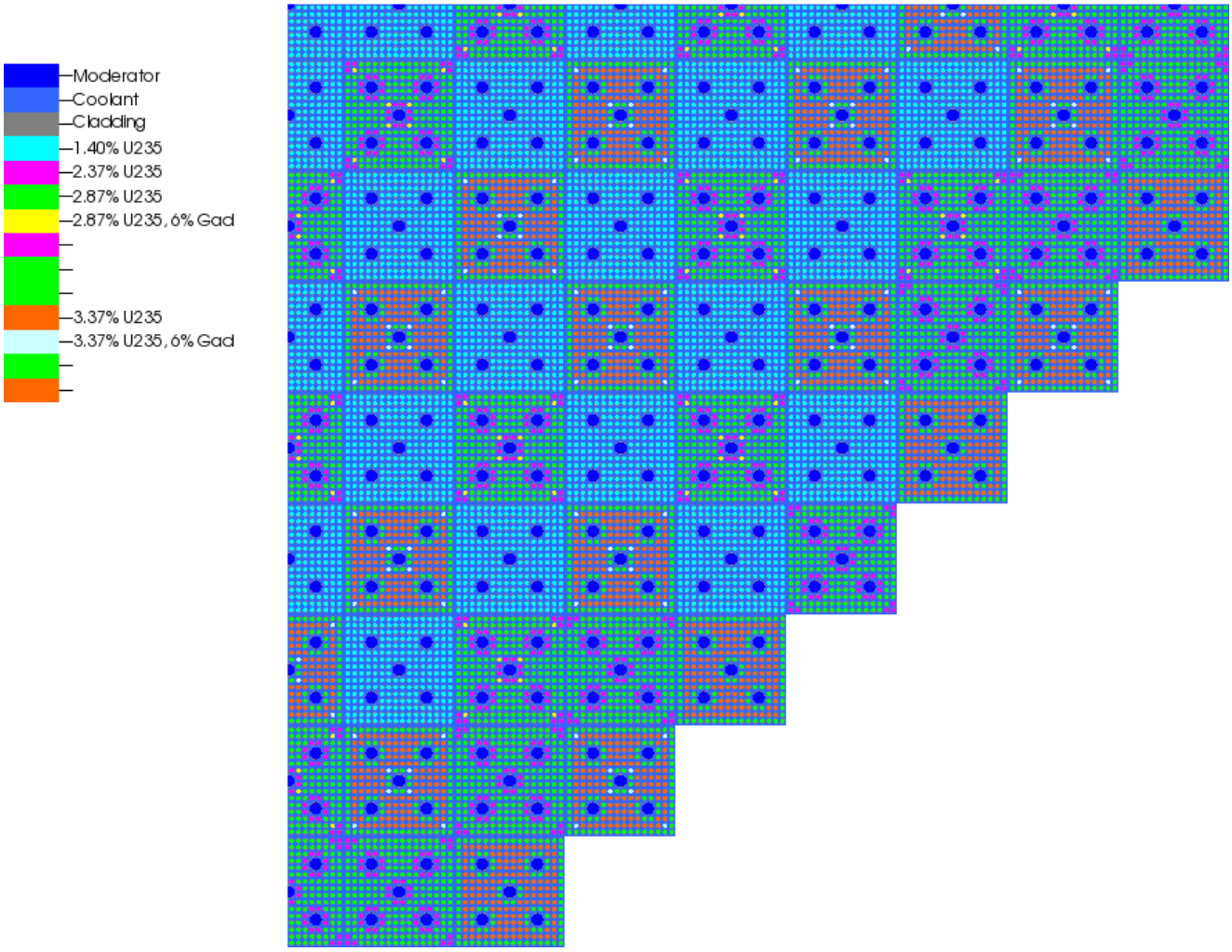

Figure 15: Modified C/E PWR Core Model

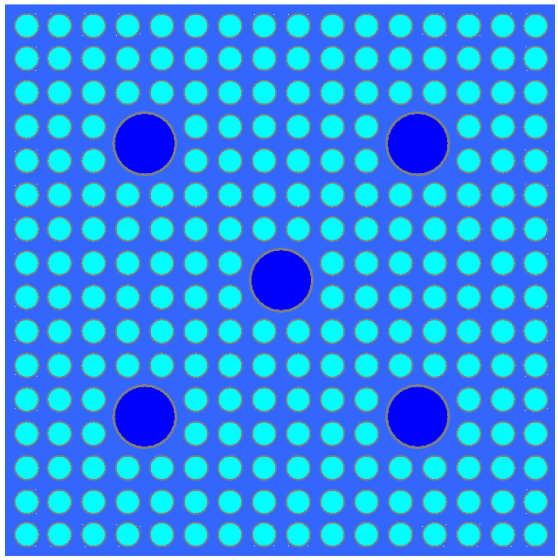

(a) Type A - 1.4% enriched

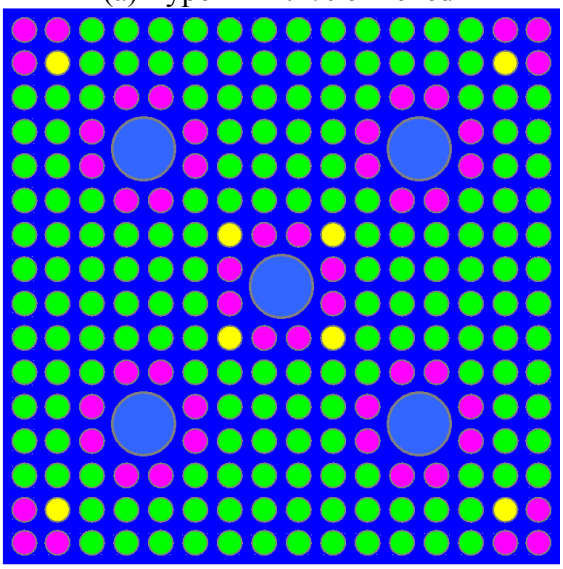

(b) Type B1 - 2.8% enriched (with Gd_2O_3)

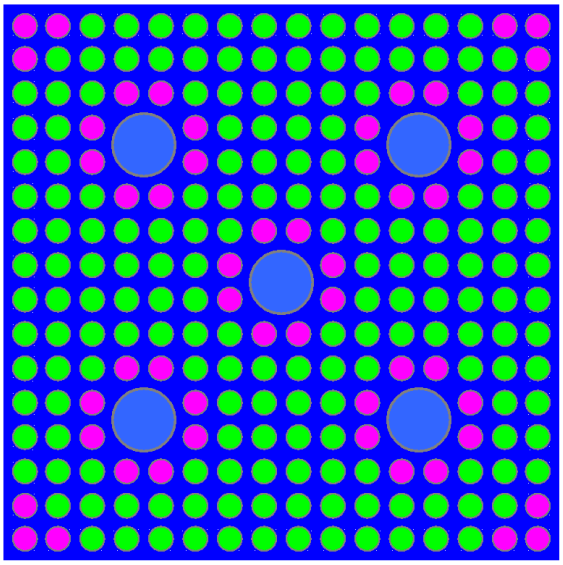

(c) Type B2 - 2.8% enriched

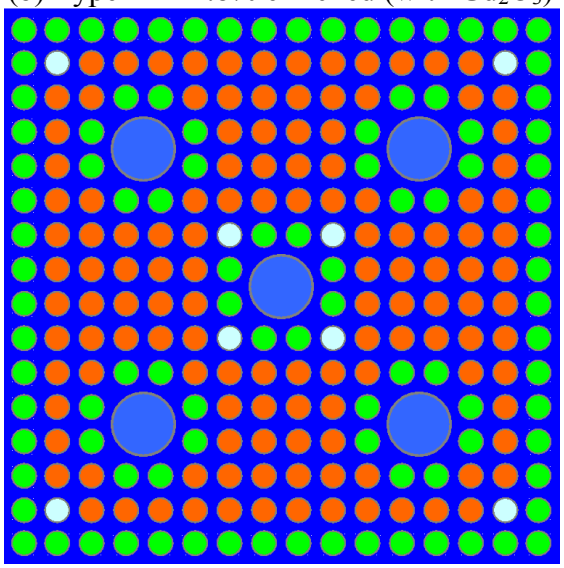

(f) Type C1 - 3.3% enriched (with Gd_2O_3)

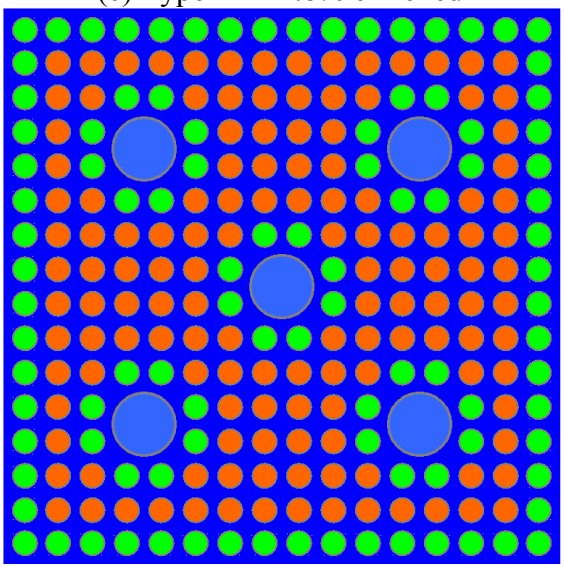

(f) Type C2 - 3.3% enriched

Figure 16: C/E Lattice Model Geometry and Mesh

In this model the MOC discretization used 0.05 cm ray spacing, and 8 azimuthal and 2 polar angles per octant with the Cheybyshev-Yamamoto angular quadrature. The cross section library used was `mpact47g_70s_v4.0_11032014.fmt`, and the scattering treatment was TCP0. The problem was run in parallel on the Falcon cluster at INL using 205 processors for full spatial decomposition. The total run time for the simulation was 2 minute and 3 seconds. The computed power distribution is shown in Figure 17.

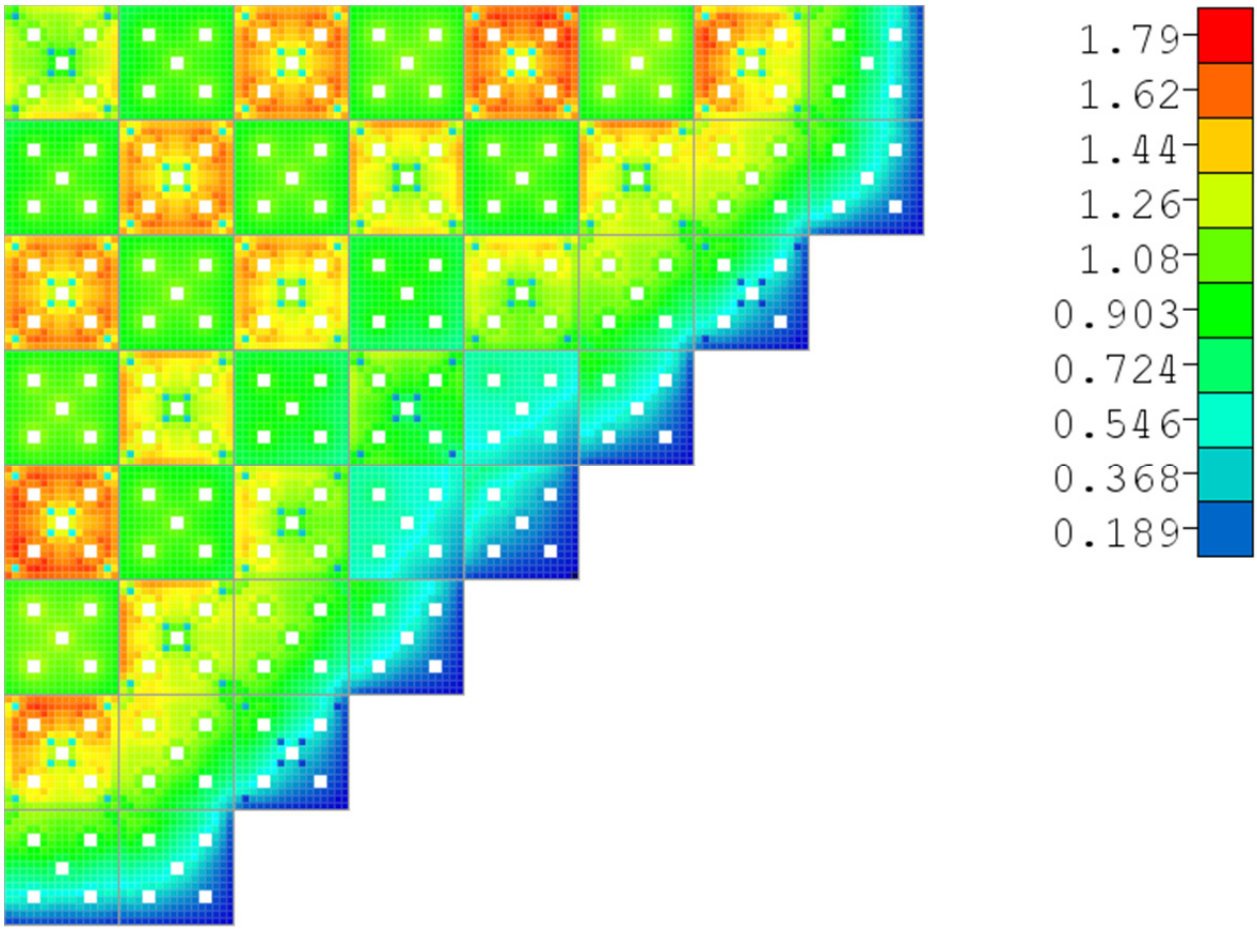

Figure 17: C/E PWR 2-D Model Powers

It is also worth noting that this simulation likely does not have a mesh refined discretization. Typically more angles are used, and the spatial mesh will need refinement in the large guide tubes. The refined spatial mesh in the guide tubes should not have a significant effect on overall run time.

5.2 2-D BWR Core Subregion

The final objective of the milestone is to demonstrate the new BWR capability on a BWR subregion. For the demonstration problem the central control cell of the Peach Bottom Unit 2 cycle 1 is used. This subregion is depicted in Figure 18.

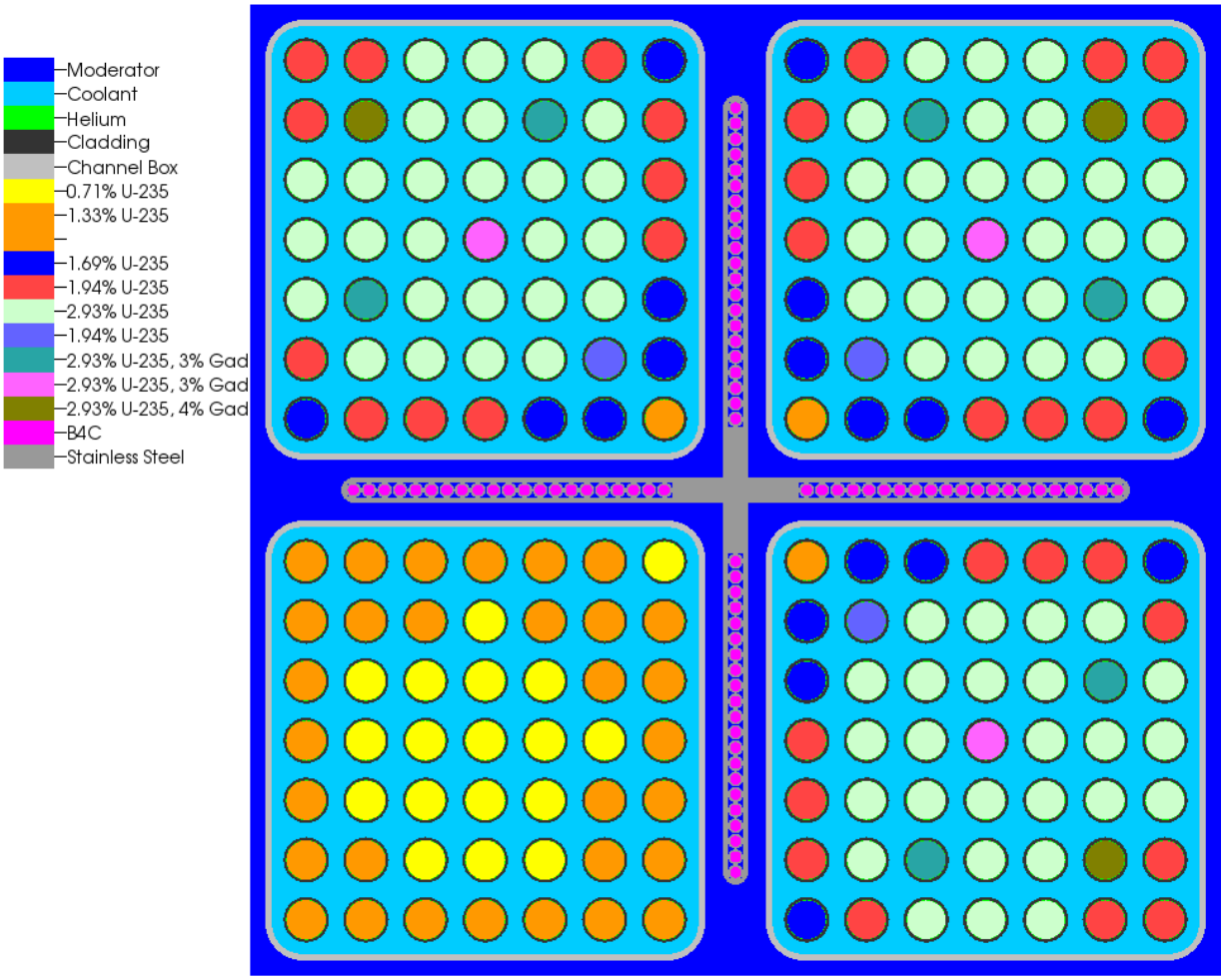

Figure 18: BWR Subregion Demonstration Problem

The model used 5 equi-volume rings in the fuel, and 2 equi-volume rings in the control blade rodlets. The MOC discretization used 0.01 cm spacing, 16 azimuthal angles and 2 polar angles per octant with the Cheybyshev-Yamamoto quadrature. The `mpact47g_70s_v4.0_11032014.fmt` library was used with P2 scattering. Simulated conditions correspond to cold zero power. The simulation was run with 4 threads on a workstation and converged in 9 iterations. The run time was just under 1 hour. Plots are shown below for the computed flux distribution for select energy groups.

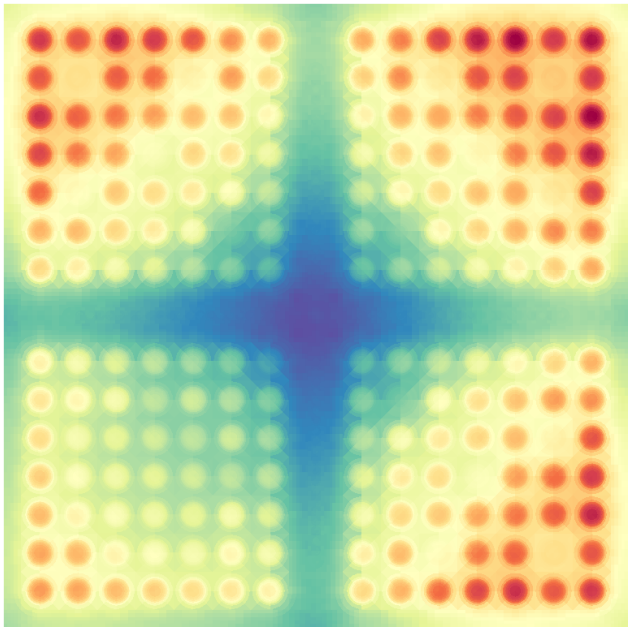

(a) Flux distribution in Group 1
(20 MeV - 6.0653 MeV)

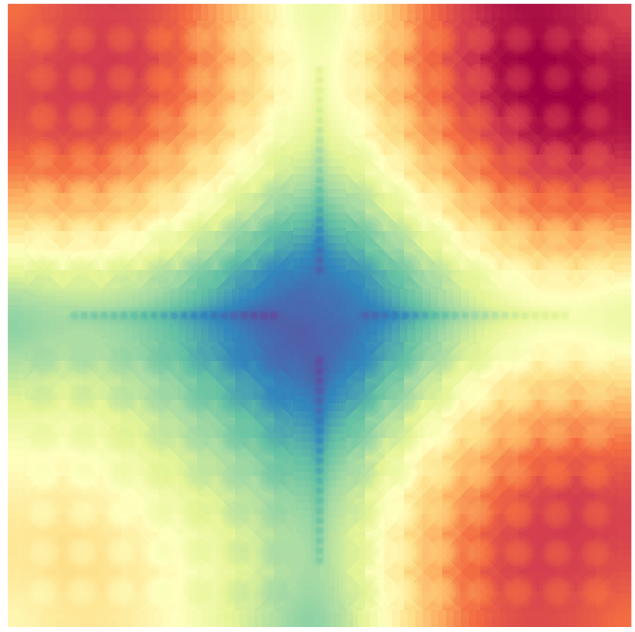

(b) Flux distribution in Group 10
(9.12 keV - 2.03 keV)

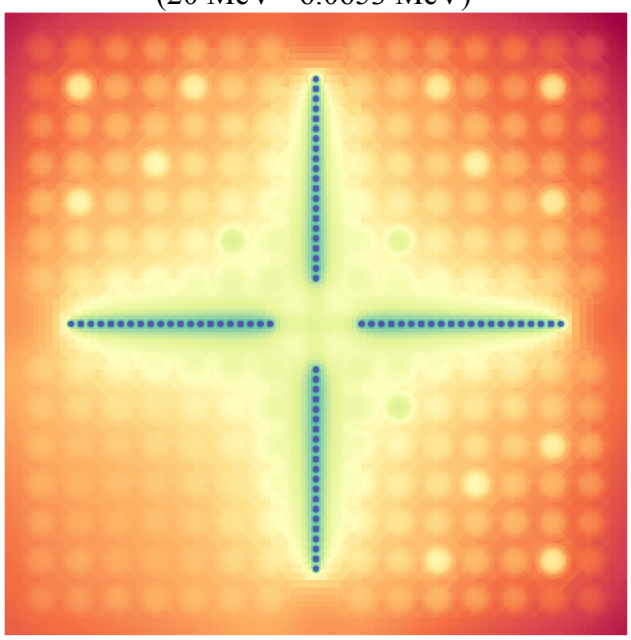

(c) Flux Distribution in Group 37
(0.50323 eV - 0.35767 ev)

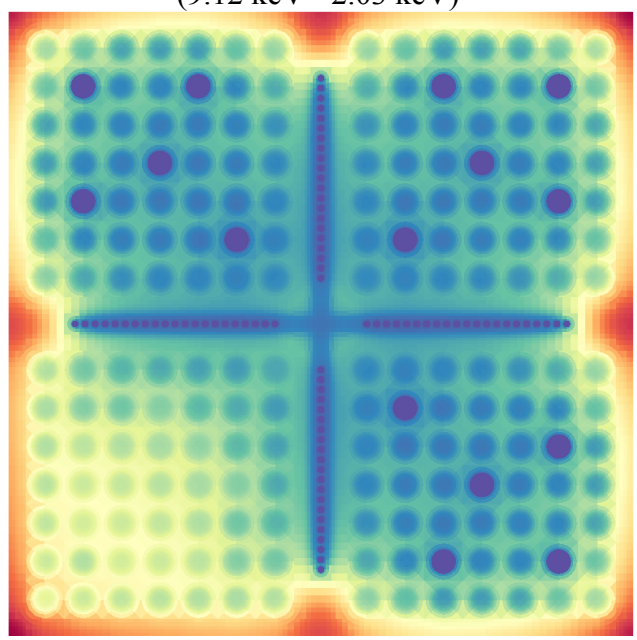

(d) Flux distribution in Group 47
(< 0.012396 eV)

Figure 19: Flux Distributions for BWR subregion

5.3 Progress on ATRIUM-10 Assembly (Stretch Goal)

Another stretch goal within this milestone was the simulation of an ATRIUM-10 bundle design. Some progress towards this goal was achieved; however, it was not strictly met. The goal was to simulate this bundle design using the VERA input, however, the VERA input has not yet been developed to describe the ATRIUM-10 water box.

Nevertheless, specifications for an ATRIUM-10 like bundle design exist [11] and a model for this problem was developed using MPACT's native input, which in some ways is more general, but far

less user friendly than the VERA input. It is also noted that this model does not specify the corner radii for the channel box or water box, thus its geometry is still an approximation to the physical bundle design. The model geometry is shown in Figure 20

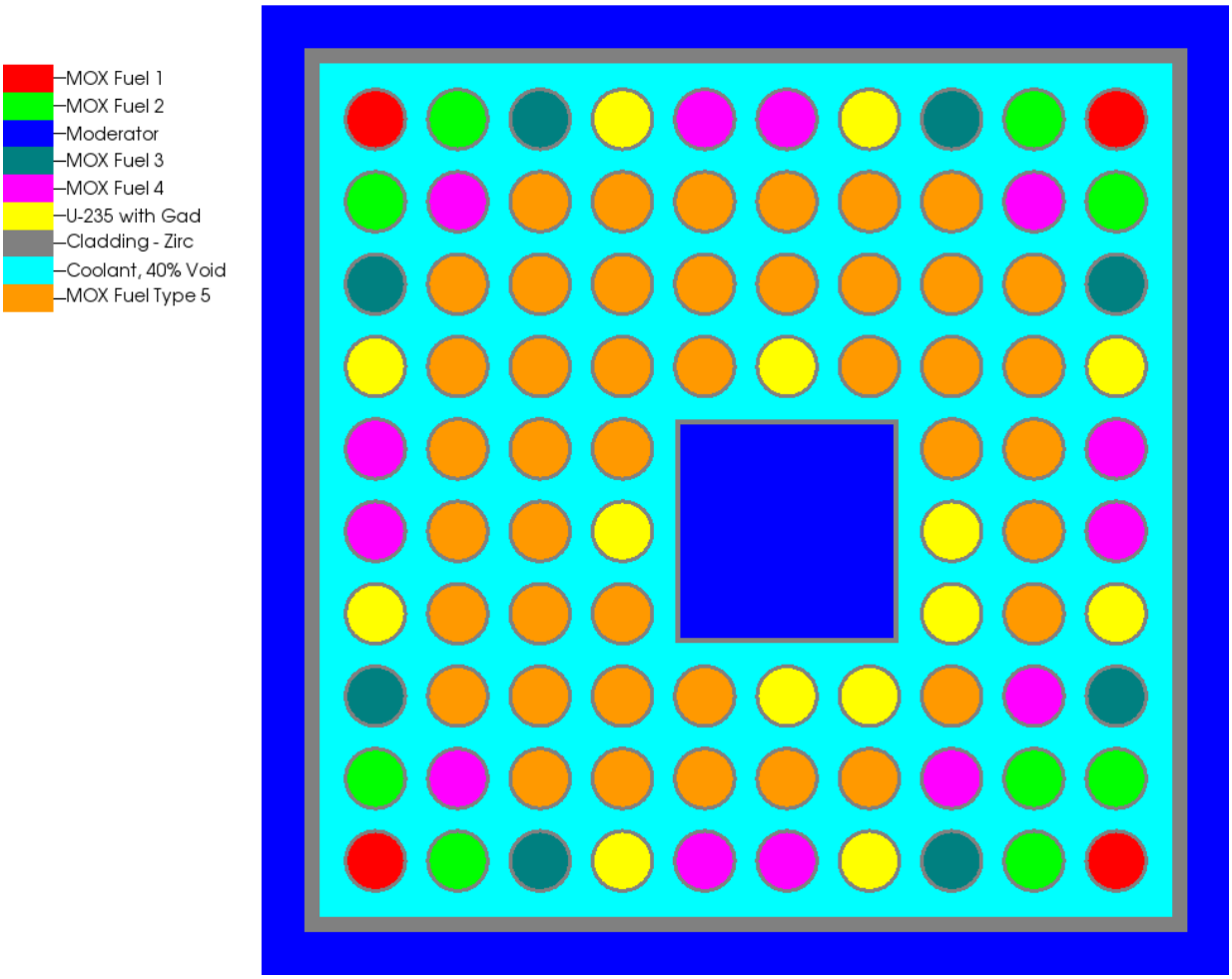

Figure 20: BWR MOX Assembly MPACT Model from "Benchmark Problem Suite for Reactor Physics Study of LWR Next Generation Fuels" [11].

The model was discretized with 0.03 cm ray spacing, 16 azimuthal angles, and 3 polar angles per octant using the Chebyshev-Yamamoto angular quadrature. The cross section library used was `mpact47g_e70r0_TCP0.xsl`, and the scattering treatment was TCP0. The computed flux distributions from this model are shown for select groups in Figure 21.

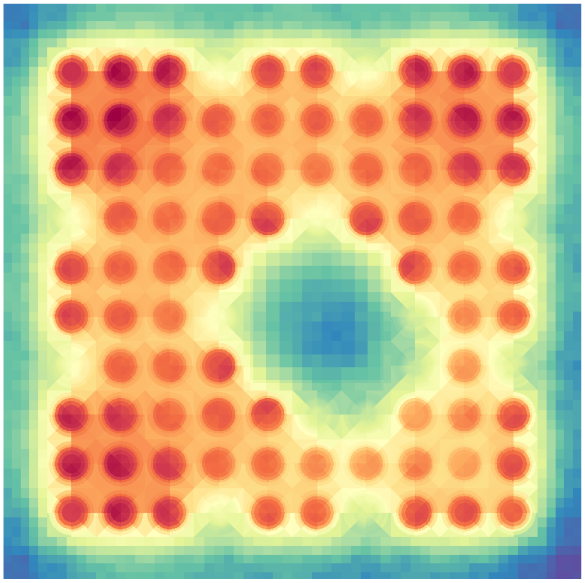

(a) Flux distribution in Group 1
(20 MeV - 6.0653 MeV)

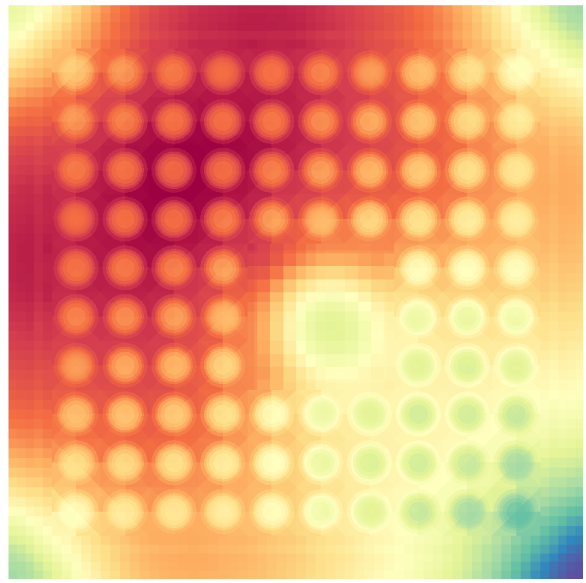

(b) Flux distribution in Group 10
(9.12 keV - 2.03 keV)

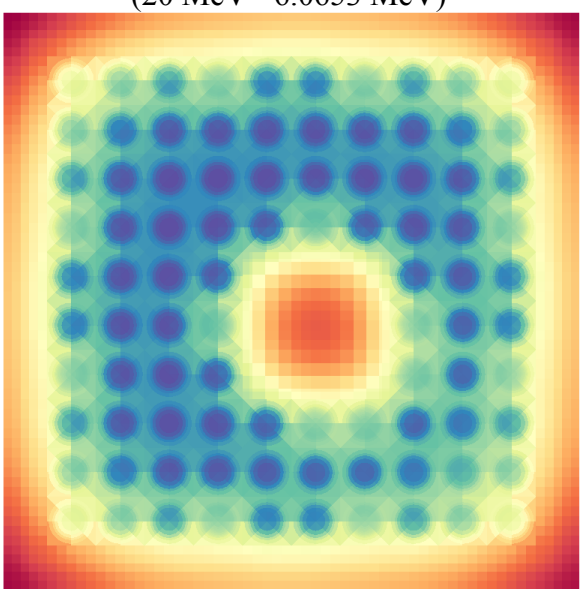

(c) Flux Distribution in Group 37
(0.50323 eV - 0.35767 ev)

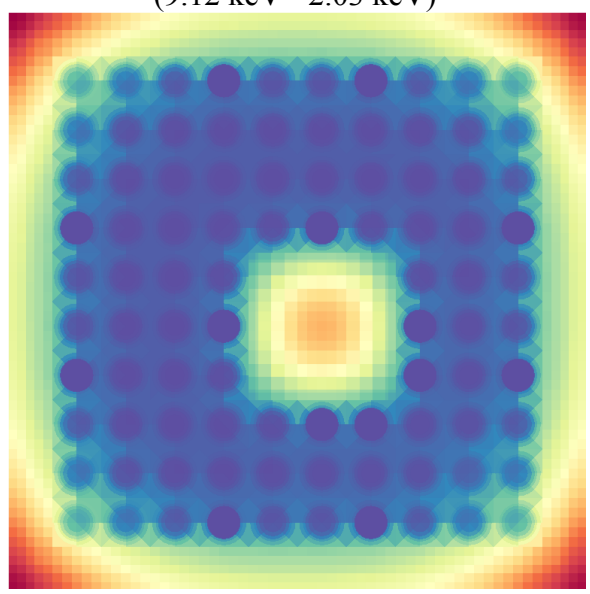

(d) Flux distribution in Group 47
(< 0.012396 eV)

Figure 21: Flux Distributions for ATRIUM-10 Lattice

5.4 3-D Assembly (Stretch Goal)

One of the stretch goals for this milestone was to simulate a single 3-D BWR assembly. To demonstrate the progress towards having the capability for this stretch goal, the GE-12 lattice described in section 5.1.1 was extended to 3-D and made to include an upper region with vanished rods, the location of which also comes from [2]. The 3-D bundle design was also given 6" natural uranium blankets at the top and bottom and an upper plenum region was defined with a height consistent with what was given in [5]. The images of this model are shown in Figure 22. This model did not include any tie plates, axial reflectors or core plates. When these model features were attempted, it was discovered that they were not yet fully functional for BWR geometry, thus enabling 3-D modeling is still an area of ongoing work.

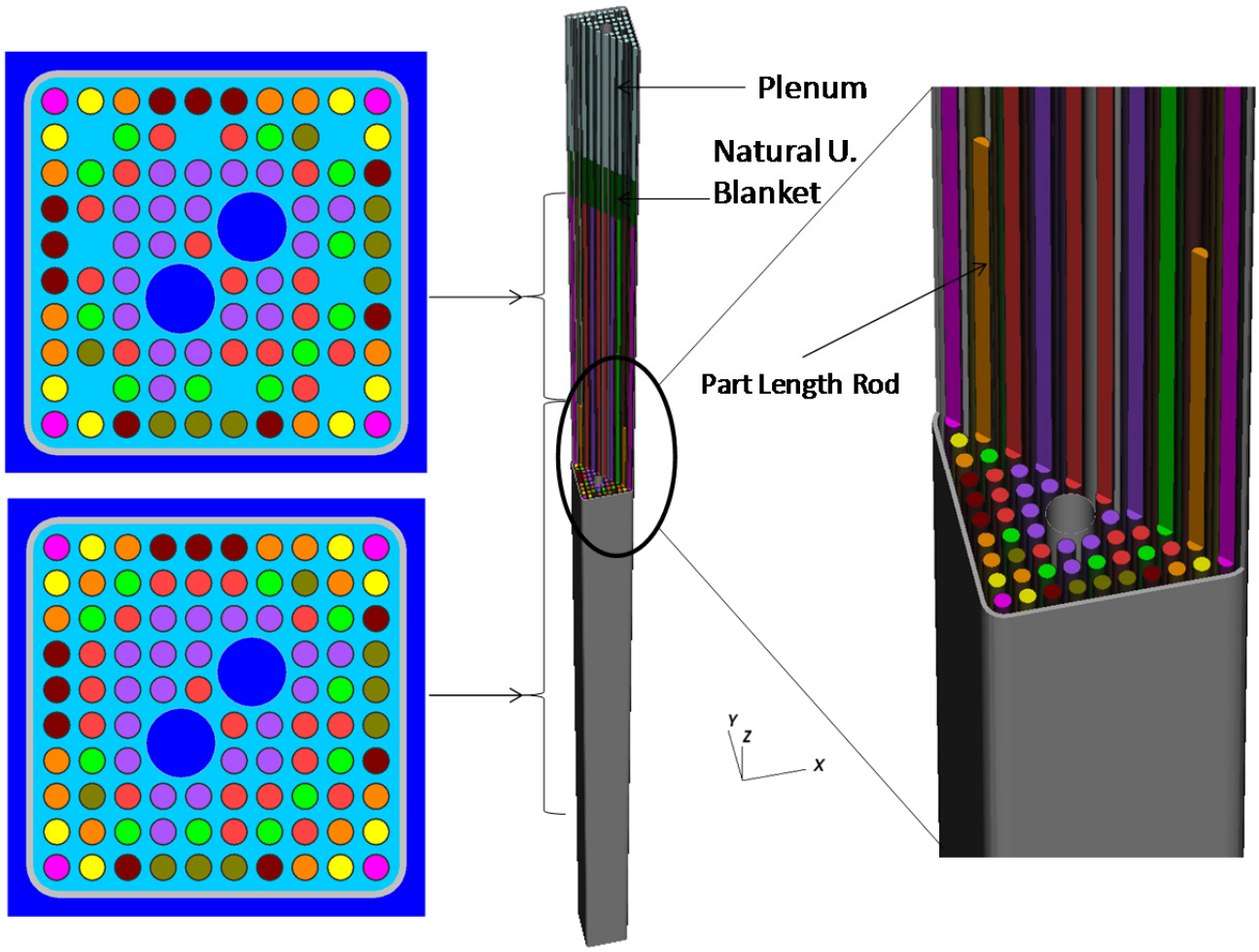

Figure 22: Visualization of MPACT Geometry for 3-D BWR Assembly

The model was simulated at hot conditions with 0% void. The model had an MOC discretization of 0.05 cm ray spacing, 8 azimuthal angles and 2 polar angles per octant using the Chebyshev-Yamamoto quadrature. The cross section library used was `mpact47g_70s_v4.0_11032014.fmt`, and the scattering treatment was P2. The model was discretized into 3" nodes axially for all fuel lattices, and into 4" nodes in the plenum region. The axial mesh consisted of 52 total planes. The simulation was run in parallel on the Fission cluster at INL using 52 processors for full spatial decomposition. The total run time of the simulation was 4 minutes and 43 seconds. The convergence criteria for the eigenvalue and flux were set to 1.0e-6 and these criteria were reached after 9 iterations. The computed 3-D power distribution is shown in Figure 23.

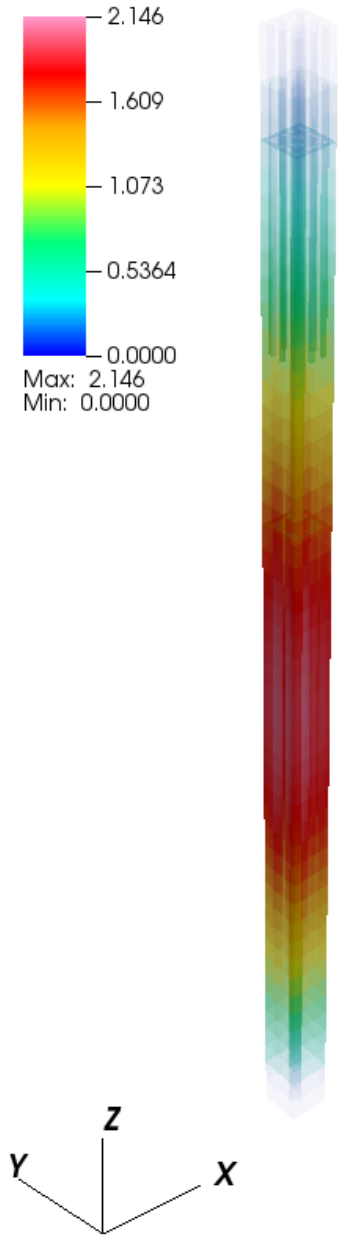

Figure 23: Computed Relative Power Distribution for 3-D BWR Assembly

5.5 Peach Bottom Beginning of Cycle 1 2-D (Stretch Goal)

As another stretch goal that was not specifically defined in [3] but which was addressed here was to build a full core 2-D model of Peach Bottom Unit 2, Cycle 1 without control blades. This model was successfully meshed by MPACT, and the resulting geometry is shown in Figure 24. The cycle 1 loading pattern was obtained from [12].

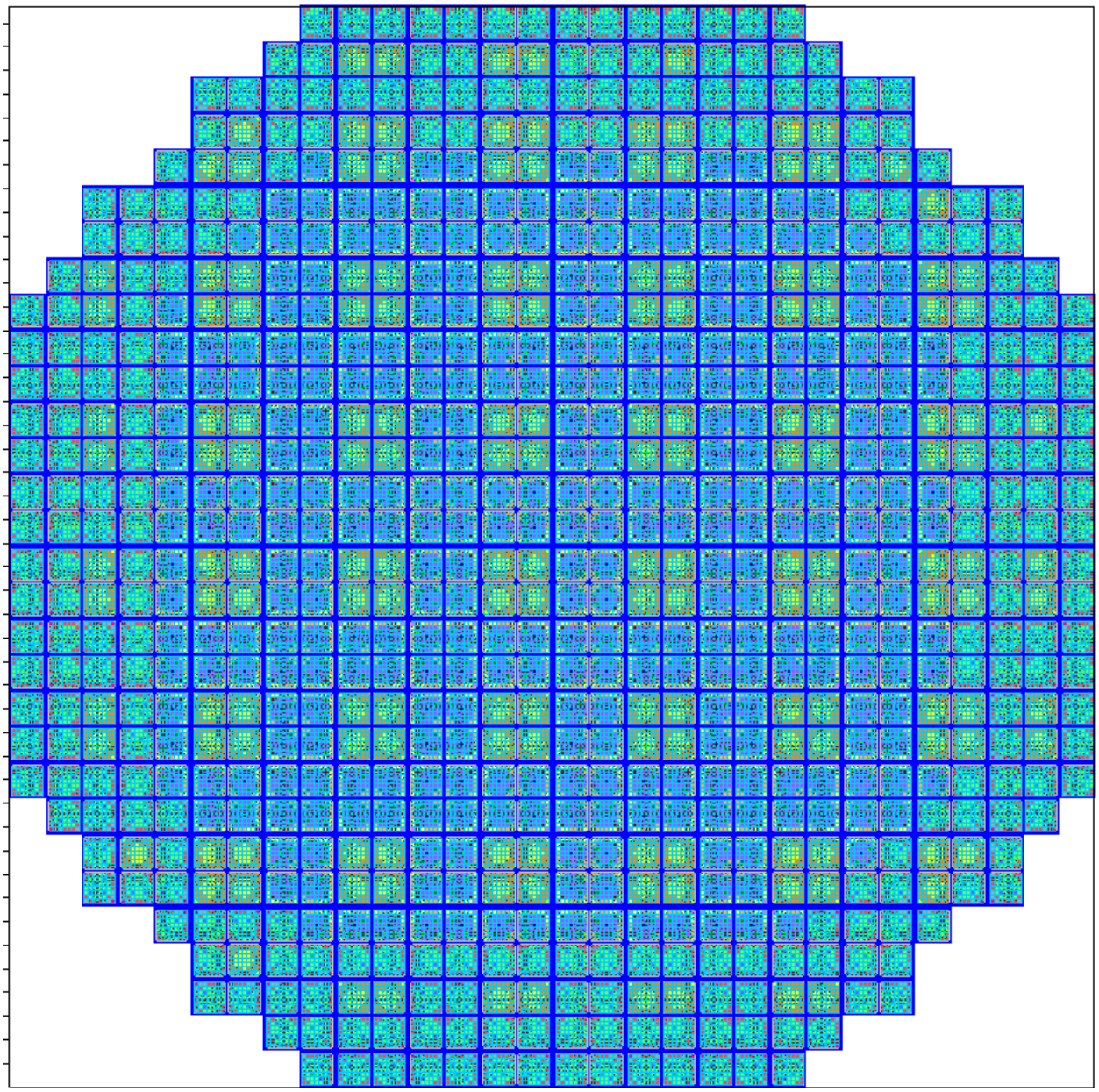

Figure 24: Full Core Peach Bottom Unit 2 Beginning of Cycle 1 (2-D)

In this model the MOC discretization used 0.05 cm ray spacing, and 8 azimuthal and 2 polar angles per octant with the Cheybyshev-Yamamoto angular quadrature. The cross section library used was `mpact47g_70s_v4.0_11032014.fmt`, and the scattering treatment was P2. The problem was run in parallel on the Falcon cluster at INL using 764 processors, one for each assembly, for full spatial decomposition. The total run time of the simulation was 7 minutes and 44 seconds. The convergence criteria for the eigenvalue and flux were set to 1.0e-6 and these criteria were reached after 14 iterations. The computed 2-D power distribution is shown in

Figure 25.

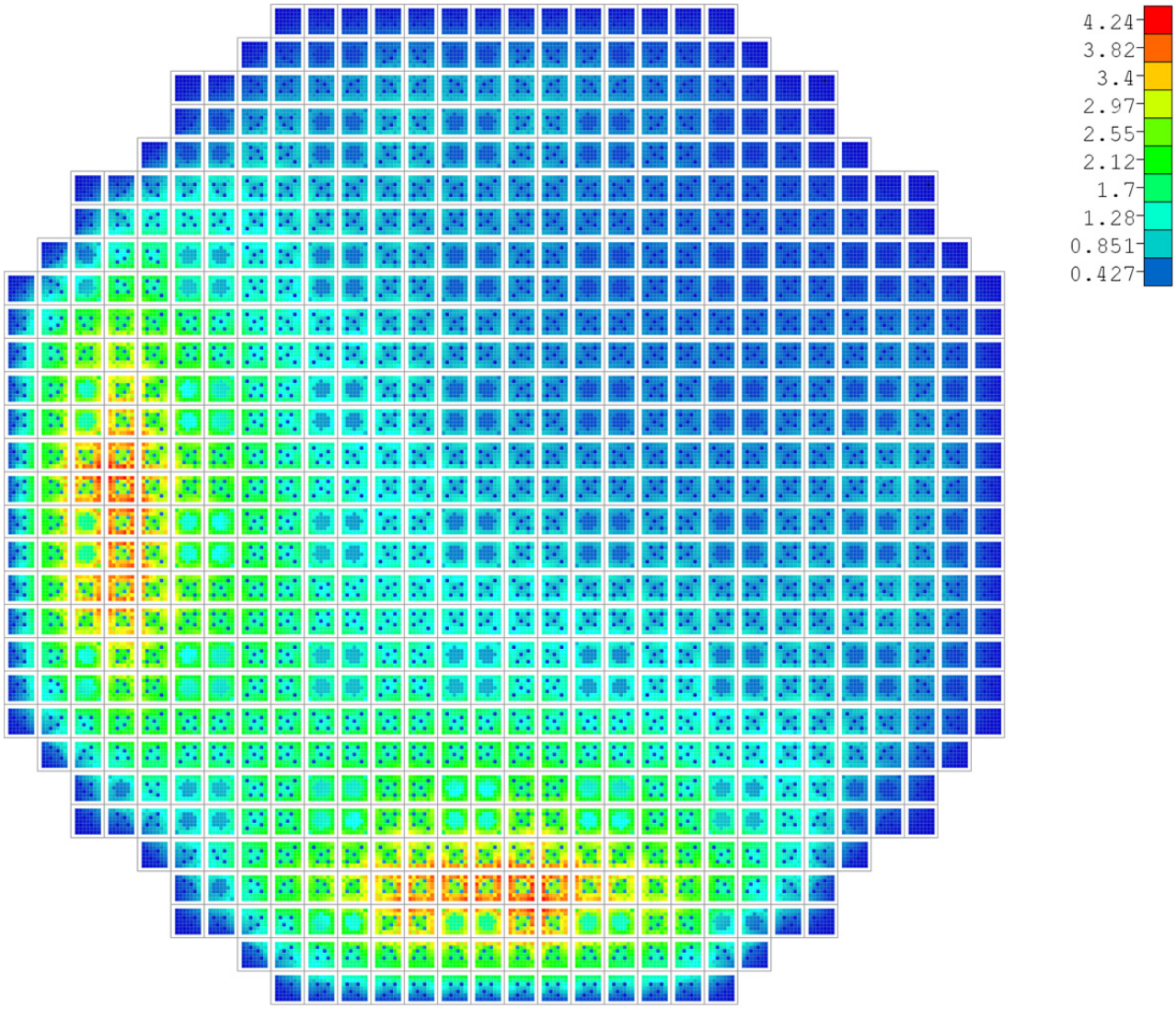

Figure 25: Peach Bottom Unit 2 BOC1 CZP Power Distribution (2-D)

6. CONCLUSIONS AND FUTURE WORK

This milestone report described the initial effort on one of the priorities for Phase II of CASL which is the extension of the VERA-CS LWR modeling capability to the BWR. The specific focus of the work reported here was on the extension of the capability of the neutronics code MPACT to BWR geometry. Modifications to the code were performed to treat the defining neutronics characteristics of a BWR geometry compared to a PWR, which included the presence of a channel box around the fuel pins to separate the coolant flow around the fuel and the presence of large water channels in the fuel pin lattices. The detailed scope and objectives of this milestone were developed in a preceding milestone, L3:PHI.VCS.P10.02 for the "Initial BWR Input Specifications". As defined in the specifications, the initial capability targeted for BWR applications in VERA-CS was

(1) Channel box with rounded corners
(2) Wide and narrow gaps on the outside of the channel box
(3) Ability to specify different void/density and outside the channel box
(4) GE Original Equipment Manufacturer (OEM) control blade design
(5) Large water rods that occupy 2x2 pin cells.

Some additional second priority items from the specifications included:

(1) Thick channel box corners
(2) "Square" water rods with rounded corners (Areva ATRIUM designs)
(3) Two large water rods that together replace 7 pin cell locations (GE11 designs)
(4) Large water rods that are slightly larger than 2x2 pin cells (GE9 design)

These BWR features were implemented in MPACT and some of the code metric required for the implementation are shown in Table 8.

Table 8. Project Metrics

Metric	Value
Lines of Source Added	28,875
Lines of Test Added	44,895
Number of Unit Tests Added	24
Number of Regression Tests	25
Calendar Time	5 Months

6.1 Project Outcomes

The successful completion of the milestone objectives was demonstrated using a set of BWR progression problems which were defined in the specifications provided in L3:PHI.VCS.P10.02. These problems included:

(1) Pin cell calculations at BWR conditions
(2) Peach Bottom Assemblies with no control blades
(3) Peach Bottom Assemblies with control blades
(4) Assemblies with large 2x2 water rods (generic dimensions, including both BWR and PWRs)
(5) Atrium square channel box (if time permits)
(6) 3-D assemblies with no feedback or control blade (stretch goal, only if time permits).

No new coding features were required for the pin cell calculations, but comparison of the results of these cases with Monte Carlo calculations enabled the testing of the cross section library using BWR fuel rod dimensions and void conditions. Several deficiencies were revealed in the cross sections library, particularly at high void conditions, that will be addressed in future work within RTM. The specifications for the Peach Bottom lattices were taken from an NEA benchmark and provided a problem to perform a preliminarily assessment of the accuracy of MPACT using a legacy BWR fuel assembly design. The reference simulations for the lattices were calculated using KENO and included a total of 6 lattice types over a variety of conditions. The comparison with the Monte Carlo reference showed a significant reactivity bias with increasing void, which was consistent with the pin cell comparisons, and the RMS and max power differences were somewhat larger than what has been observed between MPACT and KENO for the VERA Benchmark Progression Problem 2 PWR lattices. However, the comparisons provided confidence that the BWR geometry capability was successfully implemented in MPACT. To verify some of the error attributable to the cross section library, the MPACT models were also run with the HELIOS library and compared to the KENO results. Results are also presented in the report for progress on the stretch goals including the modeling of the C/E PWR core design, the simulation of a single 3-D BWR assembly, and the simulation of an ATRIUM-10 bundle design. However, future work is required to finalize the capability for all of the stretch goals.

6.2 Future Work

Much the capability required to perform a simulation of a BWR was successfully demonstrated as a part of this milestone. However, work is still required to improve this functionality and provide better comparisons to reference Monte Carlo calculations. The suggested future work is organized into four categories for cross section data improvements, methods improvements, modeling improvements, and miscellaneous other improvements. The suggestions for each of these categories are included in the following subsections.

6.2.1 Cross Section Data

Deficiencies in the 47-group cross section library for BWR modeling were noted in previous sections. Work is needed here to address the biases observed at high void conditions. There also may or may not be a bias in the current library related to having lower fuel to moderator ratios in the design.

6.2.2 Methods

Several methods improvements to MPACT were mentioned in previous sections, in particular for completing the stretch goals of this milestone. Some of these methodology improvements include:

- Modification to the Coarse Mesh Finite Difference (CMFD) to be able to handle unstructured grids; necessary for mixed assembly configurations
- Implementation of a Linear Source in the MOC; this method will reduce the meshing burden and improve the accuracy of the solution near the large water rods and wide and narrow gaps.
- Improved T/H coupling; many of the geometric and modeling features added are not necessarily designed to work in the existing T/H coupling framework, thus this coupling would need to be improved.

- Control rod de-cusping; this feature may not be needed for the notched control blade drives, but the newer fine motion control rod drives would require some control rod de-cusping.
- Iteration Stability; many of the underlying problem characteristics that tend to cause stability concerns in PWR analysis are generally magnified in a BWR system. Thus it is expected that additional improvements will be needed to ensure that the iterative methods employed are stable for BWR analysis as well.
- Gadolinium depletion; the depletion treatment of gadolinium is well known to be a limiting factor in the depletion step size. Methods currently exist to improve the accuracy of gadolinium depletion and thus these can be implemented in a straight-forward manner.
- Azimuthally dependent cross sections; presently the cross section mesh regions in MPACT can only have a radial spatial dependence for a given material. BWR geometries have significantly more local heterogeneity in the angular domain, which might necessitate an azimuthal dependence in the cross sections for depletion in certain applications.

6.2.3 Modeling

Several BWR features still cannot be modeled in MPACT and should be addressed in future work. Some of these features include:

- User input for meshing of the channel box and control blade
- Thick channel box corners
- Square water boxes with rounded corners
- Thick-thin and thick-thin-thin channel boxes
- Fuel rod connectors
- SVEA water cross designs
- Non-OEM control blade designs
- Assembly upper and lower tie plates
- 3-D Modeling
- Control Rod Motion
- Grid Spacers
- Detectors
- Other miscellaneous structural components in the vessel (e.g. core plate, shroud)

6.2.4 Miscellaneous

In addition to the data, methods, and modeling needs, additional work should be performed on making the BWR functionality easier for the user. Additionally, code work is necessary to generate evidence that the software is correct and that its models are sufficiently representative of the actual BWR. Much of this work would require additional testing for defect identification, followed by addressing the defects themselves. As much as testing is a priority during development, not every case is typically identified *a priori*, and therefore issues are often identified later and must be addressed to provide a robust capability to users. Code BWR validation should also be a priority and the information contained in [12] and other publicly available reports should provide sufficient detail to create models that can be evaluated against initial critical conditions and then extended to full BWR operating conditions.

REFERENCES

1. I. C. Gauld, "SCALE-4 Analysis of LaSalle Unit 1 BWR Commercial Reactor Critical Configurations," ORNL/TM-1999/247, March, (2000).
2. "Physics of Plutonium Fuels BWR MOX Benchmark Specification and Results," NEA/NSC, Volume VII, ISBN: 92-64-19905-5, January (2003).
3. Palmtag, S., "Initial Boiling Water Reactor (BWR) Input Specifications," CASL Technical Report: CASL-U-2015–0040–000, February 28, (2015).
4. E.W. Lemmon, M.O. McLinden and D.G. Friend, "Thermophysical Properties of Fluid Systems," in NIST Chemistry WebBook, NIST Standard Reference Database Number 69, Eds. P.J. Linstrom and W.G. Mallard, National Institute of Standards and Technology, Gaithersburg MD, 20899, http://webbook.nist.gov, (retrieved July 28, 2015).
5. J. Solis, K. N. Ivanov, B. Sarikaya, A. M. Olsen, and K. W. Hunt, "Boiling Water Reactor Turbine Trip Benchmark Volume I: Final Specifications," NEA/NSC/DOC(2001)1
6. SCALE: A Modular Code System for Performing Standardized Computer Analyses for Licensing Evaluation, ORNL-TM/2005/39, Version 6, Vols. I–III, Oak Ridge National Laboratory, Oak Ridge, Tenn. (2009). (Available from Radiation Safety Information Computational Center at Oak Ridge National Laboratory as CCC-750.)
7. A. Godfrey, "MPACT Testing and Benchmarking Results," CASL Technical Report, CASL-2014-0045-000, March, 31, (2014).
8. C.A. Wemple, H-N.M. Gheorghiu, R.J.J. Stamm'ler, E.A. Villarino, "The HELIOS-2 Lattice Physics Code," 18th AER Symposium on VVER Reactor Physics and Reactor Safety.
9. B. Kochunas, T. Downar, R. Brewster and E. Baglietto, "Full-core 3D MOC Transport (2D/1D, Pin-resolved) Capability with T-H Coupling," CASL Technical Report: CASL-U-2011–0075–000, June 30, (2011).
10. D. J. Kelly, "Depletion of a BWR Lattice Using the RACER Continuous Energy Monte Carlo Code," Proc. Int. Conf. on Math and Comp., Reactor Physics, and Env. Analysis, Portland, Oregon, USA, April 30-May 4 (1995).
11. A. Yamamoto, T. Ikehara, T. Ito, and E. Saji, "Benchmark Problem Suite for Reactor Physics Study of LWR Next Generation Fuels", *Nucl. Sci. Tech.*, Technical Report, **39**, 8, pp. 900-912, August (2002).
12. N.H. Larsen, "Core Design and Operating Data for Cycles 1 and 2 of Peach Bottom 2," EPRI Technical Report, NP-563, June, (1978).

APPENDIX A - DETAILED PEACH BOTTOM LATTICE COMPARISONS

This appendix contains the detailed comparisons for the lattices simulated as a part of Section 4 of this report. All simulations in MPACT used the same discretization, which are given in Section 4. The only differences between the sets of results given here are the cross section library and scattering treatment option. Table A.1 through A.6 give the comparisons between MPACT and KENO for the `mpact47g_70s_v4.0_11032014.fmt` library with P2 scattering. Table A7. through A.12 show comparisons to the same reference KENO results, but the MPACT results were generated using the HELIOS library and P2 scattering. The last set of tables, A.13 through A.18 show comparisons between MPACT using the `mpact47g_70s_v4.0_11032014.fmt` library and TCP0 scattering KENO.

In all tables the comparison values were computed as MPACT - KENO

Table A.1. MPACT and KENO Comparisons for Peach Bottom Lattices at CZP (unrodded, ORNL P2)

Lattice	KENO k-eff	MPACT Δk-eff (pcm)	Pin Power Max. Absolute Difference	Pin Power RMS
Type 1	1.02682 (±2 pcm)	65	1.77%	0.62%
Type 2	1.11948 (±2 pcm)	-138	2.54%	1.11%
Type 3	1.06720 (±2 pcm)	-282	2.86%	1.21%
Type 4 (100-mil channel)	1.12751 (±2 pcm)	-173	2.52%	0.95%
Type 4 (120-mil channel)	1.12877 (±2 pcm)	-204	2.36%	0.94%
Type 5	1.13445 (±2 pcm)	-142	2.37%	0.96%
Type 6	1.13103 (±2 pcm)	-190	2.34%	0.94%

Table A.2. MPACT and KENO Comparisons for Peach Bottom Lattices at HZP (unrodded, ORNL P2)

Lattice	KENO k-eff	MPACT Δk-eff (pcm)[a]	Pin Power Max. Absolute Difference	Pin Power RMS
Type 1	1.04770 (±2 pcm)	529	0.83%	0.28%
Type 2	1.10536 (±2 pcm)	-211	1.50%	0.73%
Type 3	1.04024 (±2 pcm)	-215	1.66%	0.78%
Type 4 (100-mil channel)	1.10087 (±2 pcm)	-106	1.45%	0.63%
Type 4 (120-mil channel)	1.09890 (±2 pcm)	-113	1.43%	0.62%
Type 5	1.11378 (±2 pcm)	-59	1.53%	0.64%
Type 6	1.11257 (±2 pcm)	-110	1.35%	0.60%

Table A.3. MPACT and KENO Comparisons for Peach Bottom Lattices at 0% Void (unrodded, ORNL P2)

Lattice	KENO k-eff	MPACT Δk-eff (pcm)[a]	Pin Power Max. Absolute Difference	Pin Power RMS
Type 1	1.04770 (±2 pcm)	-45	0.79%	0.28%
Type 2	1.09904 (±2 pcm)	-172	1.50%	0.72%
Type 3	1.03423 (±2 pcm)	-179	1.63%	0.76%
Type 4 (100-mil channel)	1.09440 (±2 pcm)	-68	1.43%	0.61%
Type 4 (120-mil channel)	1.09233 (±2 pcm)	-75	1.40%	0.60%
Type 5	1.10736 (±2 pcm)	-26	1.45%	0.62%
Type 6	1.10629 (±2 pcm)	-65	1.37%	0.58%

Table A.4. MPACT and KENO Comparisons for Peach Bottom Lattices at CZP (rodded, ORNL P2)

Lattice	KENO k-eff	MPACT Δk-eff (pcm)[a]	Pin Power Max. Absolute Difference	Pin Power RMS
Type 1	0.84993 (±2 pcm)	-283	0.93%	0.45%
Type 2	0.93902 (±2 pcm)	-294	2.12%	0.81%
Type 3	0.89800 (±2 pcm)	-357	2.06%	0.84%
Type 4 (100-mil channel)	0.95841 (±2 pcm)	-287	2.43%	0.76%
Type 4 (120-mil channel)	0.95751 (±3 pcm)	-311	2.05%	0.69%
Type 5	0.96470 (±3 pcm)	-250	2.41%	0.76%
Type 6	0.96482 (±2 pcm)	-312	1.59%	0.62%

Table A.5. MPACT and KENO Comparisons for Peach Bottom Lattices at HZP (rodded, ORNL P2)

Lattice	KENO k-eff	MPACT Δk-eff (pcm)[a]	Pin Power Max. Absolute Difference	Pin Power RMS
Type 1	0.78854 (±2 pcm)	-137	0.64%	0.31%
Type 2	0.85967 (±2 pcm)	-28	1.30%	0.57%
Type 3	0.81708 (±3 pcm)	-16	1.41%	0.60%
Type 4 (100-mil channel)	0.87627 (±3 pcm)	35	1.44%	0.51%
Type 4 (120-mil channel)	0.87370 (±3 pcm)	28	1.10%	0.42%
Type 5	0.88651 (±2 pcm)	68	1.40%	0.50%
Type 6	0.88728 (±3 pcm)	-66	1.59%	0.57%

Table A.6. MPACT and KENO Comparisons for Peach Bottom Lattices at 0% Void (rodded, ORNL P2)

Lattice	KENO k-eff	MPACT Δk-eff (pcm)[a]	Pin Power Max. Absolute Difference	Pin Power RMS
Type 1	0.78317 (±2 pcm)	-81	0.63%	0.31%
Type 2	0.85443 (±2 pcm)	7	1.29%	0.57%
Type 3	0.81203 (±2 pcm)	21	1.36%	0.58%
Type 4 (100-mil channel)	0.87082 (±2 pcm)	70	1.38%	0.48%
Type 4 (120-mil channel)	0.86815 (±3 pcm)	67	1.06%	0.42%
Type 5	0.88107 (±3 pcm)	101	1.36%	0.48%
Type 6	0.88195 (±3 pcm)	-35	1.60%	0.56%

Table A.7. MPACT and KENO Comparisons for Peach Bottom Lattices at CZP (unrodded, HELIOS P2)

Lattice	KENO k-eff	MPACT Δk-eff (pcm)[a]	Pin Power Max. Absolute Difference	Pin Power RMS
Type 1	1.02682 (±2 pcm)	-3	0.89%	0.33%
Type 2	1.11948 (±2 pcm)	-97	1.64%	0.65%
Type 3	1.06720 (±2 pcm)	-144	1.85%	0.72%
Type 4 (100-mil channel)	1.12751 (±2 pcm)	-86	1.45%	0.50%
Type 4 (120-mil channel)	1.12877 (±2 pcm)	-100	1.38%	0.50%
Type 5	1.13445 (±2 pcm)	-62	1.32%	0.50%
Type 6	1.13103 (±2 pcm)	-107	1.34%	0.51%

Table A.8. MPACT and KENO Comparisons for Peach Bottom Lattices at HZP (unrodded, HELIOS P2)

Lattice	KENO k-eff	MPACT Δk-eff (pcm)[a]	Pin Power Max. Absolute Difference	Pin Power RMS
Type 1	1.04770 (±2 pcm)	636	0.23%	0.09%
Type 2	1.10536 (±2 pcm)	7	0.57%	0.31%
Type 3	1.04024 (±2 pcm)	31	0.67%	0.35%
Type 4 (100-mil channel)	1.10087 (±2 pcm)	81	0.43%	0.22%
Type 4 (120-mil channel)	1.09890 (±2 pcm)	82	0.46%	0.23%
Type 5	1.11378 (±2 pcm)	103	0.45%	0.23%
Type 6	1.11257 (±2 pcm)	49	0.39%	0.20%

Table A.9. MPACT and KENO Comparisons for Peach Bottom Lattices at 0% Void (unrodded, HELIOS P2)

Lattice	KENO k-eff	MPACT Δk-eff (pcm)[a]	Pin Power Max. Absolute Difference	Pin Power RMS
Type 1	1.04770 (±2 pcm)	-45	0.28%	0.11%
Type 2	1.09904 (±2 pcm)	-56	0.59%	0.34%
Type 3	1.03423 (±2 pcm)	-39	0.65%	0.37%
Type 4 (100-mil channel)	1.09440 (±2 pcm)	18	0.48%	0.25%
Type 4 (120-mil channel)	1.09233 (±2 pcm)	21	0.46%	0.25%
Type 5	1.10736 (±2 pcm)	40	0.51%	0.25%
Type 6	1.10629 (±2 pcm)	-7	0.45%	0.23%

Table A.10. MPACT and KENO Comparisons for Peach Bottom Lattices at CZP (rodded, HELIOS P2)

Lattice	KENO k-eff	MPACT Δk-eff (pcm)[a]	Pin Power Max. Absolute Difference	Pin Power RMS
Type 1	0.84993 (±2 pcm)	-179	1.38%	0.52%
Type 2	0.93902 (±2 pcm)	-218	2.23%	0.73%
Type 3	0.89800 (±2 pcm)	-240	2.56%	0.78%
Type 4 (100-mil channel)	0.95841 (±2 pcm)	-202	2.18%	0.61%
Type 4 (120-mil channel)	0.95751 (±3 pcm)	-196	2.07%	0.61%
Type 5	0.96470 (±3 pcm)	-174	2.17%	0.62%
Type 6	0.96482 (±2 pcm)	-253	1.92%	0.62%

Table A.11. MPACT and KENO Comparisons for Peach Bottom Lattices at HZP (rodded, HELIOS P2)

Lattice	KENO k-eff	MPACT Δk-eff (pcm)[a]	Pin Power Max. Absolute Difference	Pin Power RMS
Type 1	0.78854 (±2 pcm)	98	0.77%	0.34%
Type 2	0.85967 (±2 pcm)	100	1.09%	0.44%
Type 3	0.81708 (±3 pcm)	106	1.23%	0.46%
Type 4 (100-mil channel)	0.87627 (±3 pcm)	136	0.94%	0.35%
Type 4 (120-mil channel)	0.87370 (±3 pcm)	138	0.84%	0.33%
Type 5	0.88651 (±2 pcm)	151	0.90%	0.35%
Type 6	0.88728 (±3 pcm)	65	0.85%	0.33%

Table A.12. MPACT and KENO Comparisons for Peach Bottom Lattices at 0% Void (rodded, HELIOS P2)

Lattice	KENO k-eff	MPACT Δk-eff (pcm)[a]	Pin Power Max. Absolute Difference	Pin Power RMS
Type 1	0.78317 (±2 pcm)	48	0.75%	0.35%
Type 2	0.85443 (±2 pcm)	42	1.12%	0.46%
Type 3	0.81203 (±2 pcm)	49	1.35%	0.47%
Type 4 (100-mil channel)	0.87082 (±2 pcm)	81	1.00%	0.35%
Type 4 (120-mil channel)	0.86815 (±3 pcm)	88	0.91%	0.35%
Type 5	0.88107 (±3 pcm)	98	0.97%	0.36%
Type 6	0.88195 (±3 pcm)	18	0.87%	0.33%

Table A.13. MPACT and KENO Comparisons for Peach Bottom Lattices at CZP (unrodded, ORNL TCP0)

Lattice	KENO k-eff	MPACT Δk-eff (pcm)[a]	Pin Power Max. Absolute Difference	Pin Power RMS
Type 1	1.02682 (±2 pcm)	-69	2.07%	0.70%
Type 2	1.11948 (±2 pcm)	-200	3.04%	1.34%
Type 3	1.06720 (±2 pcm)	-282	3.33%	1.46%
Type 4 (100-mil channel)	1.12751 (±2 pcm)	-172	2.97%	1.21%
Type 4 (120-mil channel)	1.12877 (±2 pcm)	-197	3.00%	1.18%
Type 5	1.13445 (±2 pcm)	-145	2.98%	1.21%
Type 6	1.13103 (±2 pcm)	-196	2.75%	1.13%

Table A.14. MPACT and KENO Comparisons for Peach Bottom Lattices at HZP (unrodded, ORNL TCP0)

Lattice	KENO k-eff	MPACT Δk-eff (pcm)[a]	Pin Power Max. Absolute Difference	Pin Power RMS
Type 1	1.04770 (±2 pcm)	428	0.95%	0.33%
Type 2	1.10536 (±2 pcm)	-168	1.88%	0.84%
Type 3	1.04024 (±2 pcm)	-100	2.04%	0.88%
Type 4 (100-mil channel)	1.10087 (±2 pcm)	-7	1.87%	0.76%
Type 4 (120-mil channel)	1.09890 (±2 pcm)	-7	1.82%	0.74%
Type 5	1.11378 (±2 pcm)	18	1.92%	0.75%
Type 6	1.11257 (±2 pcm)	-30	1.72%	0.70%

Table A.15. MPACT and KENO Comparisons for Peach Bottom Lattices at 0% Void (unrodded, ORNL TCP0)

Lattice	KENO k-eff	MPACT Δk-eff (pcm)[a]	Pin Power Max. Absolute Difference	Pin Power RMS
Type 1	1.04770 (±2 pcm)	-146	0.91%	0.33%
Type 2	1.09904 (±2 pcm)	-129	1.89%	0.83%
Type 3	1.03423 (±2 pcm)	-64	2.01%	0.86%
Type 4 (100-mil channel)	1.09440 (±2 pcm)	30	1.85%	0.74%
Type 4 (120-mil channel)	1.09233 (±2 pcm)	31	1.80%	0.72%
Type 5	1.10736 (±2 pcm)	51	1.85%	0.73%
Type 6	1.10629 (±2 pcm)	15	1.74%	0.69%

Table A.16. MPACT and KENO Comparisons for Peach Bottom Lattices at CZP (rodded, ORNL TCP0)

Lattice	KENO k-eff	MPACT Δk-eff (pcm)[a]	Pin Power Max. Absolute Difference	Pin Power RMS
Type 1	0.84993 (±2 pcm)	-563	2.16%	0.61%
Type 2	0.93902 (±2 pcm)	-524	3.53%	1.16%
Type 3	0.89800 (±2 pcm)	-559	3.92%	1.22%
Type 4 (100-mil channel)	0.95841 (±2 pcm)	-461	3.80%	1.05%
Type 4 (120-mil channel)	0.95751 (±3 pcm)	-463	3.59%	1.01%
Type 5	0.96470 (±3 pcm)	-436	3.76%	1.05%
Type 6	0.96482 (±2 pcm)	-529	3.40%	1.00%

Table A.17. MPACT and KENO Comparisons for Peach Bottom Lattices at HZP (rodded, ORNL TCP0)

Lattice	KENO k-eff	MPACT Δk-eff (pcm)[a]	Pin Power Max. Absolute Difference	Pin Power RMS
Type 1	0.78854 (±2 pcm)	-252	0.77%	0.29%
Type 2	0.85967 (±2 pcm)	-69	1.66%	0.63%
Type 3	0.81708 (±3 pcm)	-39	1.90%	0.67%
Type 4 (100-mil channel)	0.87627 (±3 pcm)	21	1.70%	0.52%
Type 4 (120-mil channel)	0.87370 (±3 pcm)	21	1.54%	0.47%
Type 5	0.88651 (±2 pcm)	33	1.66%	0.51%
Type 6	0.88728 (±3 pcm)	-55	1.55%	0.45%

Table A.18. MPACT and KENO Comparisons for Peach Bottom Lattices at 0% Void (rodded, ORNL TCP0)

Lattice	KENO k-eff	MPACT Δk-eff (pcm)[a]	Pin Power Max. Absolute Difference	Pin Power RMS
Type 1	0.78317 (±2 pcm)	-200	0.79%	0.30%
Type 2	0.85443 (±2 pcm)	-37	1.62%	0.63%
Type 3	0.81203 (±2 pcm)	-6	1.91%	0.65%
Type 4 (100-mil channel)	0.87082 (±2 pcm)	53	1.65%	0.49%
Type 4 (120-mil channel)	0.86815 (±3 pcm)	55	1.50%	0.47%
Type 5	0.88107 (±3 pcm)	63	1.61%	0.49%
Type 6	0.88195 (±3 pcm)	-15	1.46%	0.43%

APPENDIX B - SAMPLE GE-9 LATTICE INPUT

Below is a sample input for a GE-9 lattice. This input also includes an example of how the control blade is defined. It is from the VERAIn repository.

```
[CASEID]
  title 'Sample 2D GE9 BWR Lattice'

!-------------------------------------------------------------------
!
! *** Note that this input deck is not correct because we do not
! *** currently model the oversize GE11 water rod at this time
! *** The water rod in this input is smaller to fit in a pincell
!
! Geometry Reference:
! D. J. Kelly,
! "Depletion of a BWR Lattice Using the RACER Continuous Energy
!    Monte Carlo Code,"
! Portland, Oregon, USA, April 30-May 4 (1995).
!-----------------------------------------------------------------

[STATE]
  power    100.0
  tinlet   550 K  ! *** approximate
  tfuel    900 K
  pressure 1040   ! psia
  sym      full

  void
    40.0

!** at void 00,  rho=  0.736690 g/cc
!** at void 40,  rho=  0.457023 g/cc
!** at void 70,  rho=  0.247273 g/cc


[CORE]
  reactor_type BWR
  size   1
  apitch 15.24
  height 1.0
  rated  0.01 0.01   ! *** approximate

  core_shape
    1

  assm_map
    ASSY

  bc_rad reflecting
  bc_top reflecting
  bc_bot reflecting

  mat zirc2  6.56 zirc2
  mat zirc4  6.56 zirc4
```

```
[ASSEMBLY]
  npin   8
  ppitch 1.6256          ! pin pitch - does not include channel gaps

!*** 80 mil design
  gap    0.9525 .47498   ! wide and narrow channel gap (cm)
  channel_box  zirc4 0.2032 0.9652 0.0 0.0   ! channel dimensions


  fuel U16  10.0642 94.5 / 1.6
  fuel U20  10.0642 94.5 / 2.0
  fuel U22  10.0642 94.5 / 2.2
  fuel U24  10.0642 94.5 / 2.4
  fuel U26  10.0642 94.5 / 2.6
  fuel U28  10.0642 94.5 / 2.8
  fuel U30  10.0642 94.5 / 3.0
  fuel U36  10.0642 94.5 / 3.6
  fuel U36G  9.939  94.5 / 3.6 / gad=4.0
  fuel U38  10.0642 94.5 / 3.8
  fuel U40  10.0642 94.5 / 3.95
  fuel U40G  9.939  94.5 / 3.95 / gad=4.0

  cell  1 0.53213 0.61341 / U16  zirc2
  cell  2 0.53213 0.61341 / U20  zirc2
  cell  3 0.53213 0.61341 / U22  zirc2
  cell  4 0.53213 0.61341 / U24  zirc2
  cell  5 0.53213 0.61341 / U26  zirc2
  cell  6 0.53213 0.61341 / U28  zirc2
  cell  7 0.53213 0.61341 / U30  zirc2
  cell  8 0.53213 0.61341 / U36  zirc2
  cell  9 0.53213 0.61341 / U38  zirc2
  cell 10 0.53213 0.61341 / U40  zirc2
  cell 51 0.53213 0.61341 / U40G zirc2
  cell 52 0.53213 0.61341 / U36G zirc2

!** water rod is made smaller to fit in a pincell
!** cell WR 1.6002 1.7018 / mod zirc4
  cell WR 1.60 1.62 / mod zirc4 / large4

  lattice LAT
    1
    2  6
    4  8 10
    6 10 52 WR
    6 10 10 WR WR
    6 10 51 10 10 10
    5  9 10 51 10 51 10
    3  7  9 10 10 10  9  6

  axial ASSY 0.0 LAT 1.0
```

```
[CONTROL]
  title "GE OEM Control Blade"
  npin 8
  stroke  1.0 1      ! 2-D

  mat ss304 8.0 ss
  mat b4c   4.62   ! ** check for 70% theoretical density

  cell TUBE 0.17526 0.23876 / b4c ss304

!       ntube     span   th       rad    sheath    wing   mat
  blade 21 TUBE 12.3825 0.79248 0.39624 0.14224  1.98501  ss304

!*** TUBE must be included in map, or it will be excluded from
parameter list
  rodmap  EMPTY
     TUBE
     - -
     - - -
     - - - -
     - - - - -
     - - - - - -
     - - - - - - -
     - - - - - - - -

  axial BLADE 0.0 EMPTY 1.0

[MPACT]
  num_space      1
  num_angle      8
  num_threads    1
  mesh WR 7 1 /  8 !put 7 radial rings and 8 azi. div. in water rod

[INSILICO]
  num_blocks_i   4
  num_blocks_j   4
```